HHS Public Access

Author manuscript

Immunity. Author manuscript; available in PMC 2022 October 12.

Published in final edited form as:

Immunity. 2021 October 12; 54(10): 2372–2384.e7. doi:10.1016/j.immuni.2021.08.007.

Functional impairment of HIV-specific CD8+ T cells precedes aborted spontaneous control of viremia

David R. Collins[1,2], **Jonathan M. Urbach**[1], **Zachary J. Racenet**[1], **Umar Arshad**[1], **Karen A. Power**[1], **Ruchi M. Newman**[1], **Geetha H. Mylvaganam**[1,2], **Ngoc L. Ly**[1], **Xiaodong Lian**[1,3], **Anna Rull**[4], **Yelizaveta Rassadkina**[1,3], **Adrienne G. Yanez**[1,2], **Michael J. Peluso**[5], **Steven G. Deeks**[5], **Francesc Vidal**[4], **Mathias Lichterfeld**[1,3], **Xu G. Yu**[1,3], **Gaurav D. Gaiha**[1,6], **Todd M. Allen**[1], **Bruce D. Walker**[1,2,7,8]

[1]Ragon Institute of MGH, MIT and Harvard, Cambridge, MA, USA

[2]Howard Hughes Medical Institute, Chevy Chase, MD, USA

[3]Division of Infectious Diseases, Brigham and Women's Hospital, Boston, MA, USA

[4]Joan XXIII University Hospital, Pere Virgili Institute (IISPV), Rovira i Virgili University, Tarragona, Spain

[5]Division of HIV, Infectious Diseases and Global Medicine, University of California, San Francisco, CA, USA

[6]Division of Gastroenterology, Massachusetts General Hospital, Boston, MA, USA

[7]Institute for Medical Engineering and Sciences and Department of Biology, Massachusetts Institute of Technology, Cambridge, MA, USA

SUMMARY

Spontaneous control of HIV infection has been repeatedly linked to antiviral $CD8^+$ T cells but is not always permanent. To address mechanisms of durable and aborted control of viremia, we evaluated immunologic and virologic parameters longitudinally among 34 HIV-infected subjects with differential outcomes. Despite sustained recognition of autologous virus, HIV-specific proliferative and cytolytic T cell effector functions became selectively and intrinsically impaired prior to aborted control. Longitudinal transcriptomic profiling of functionally impaired HIV-specific $CD8^+$ T cells revealed altered expression of genes related to activation, cytokine-mediated

[8]Lead Contact (bwalker@mgh.harvard.edu).

AUTHOR CONTRIBUTIONS

Conceptualization: D.R.C., B.D.W. Methodology: D.R.C., J.M.U., K.A.P., R.M.N., G.H.M., X.L., G.D.G. Investigation: D.R.C., Z.J.R., U.A., K.A.P., G.H.M., N.L.L., X.L., Y.R., A.R., A.G.Y. Formal Analysis: D.R.C., J.M.U., R.M.N., X.L., A.R. Resources: S.G.D., M.J.P., G.D.G. Writing – Original Draft: D.R.C., B.D.W. Writing – Review and Editing: All authors. Funding Acquisition: B.D.W., D.R.C., T.M.A., F.V., S.G.D. X.G.Y., M.L. Supervision: B.D.W., T.M.A., X.G.Y., M.L., F.V.

DECLARATION OF INTERESTS

The authors declare no competing interests.

SUPPLEMENTAL INFORMATION

signaling and cell cycle regulation, including increased expression of the antiproliferative transcription factor *KLF2*, but not of genes associated with canonical exhaustion. Lymphoid HIV-specific CD8$^+$ T cells also exhibited poor functionality during aborted control relative to durable control. Our results identify selective functional impairment of HIV-specific CD8$^+$ T cells as prognostic of impending aborted HIV control, with implications for clinical monitoring and immunotherapeutic strategies.

eTOC BLURB

Functional HIV cure strategies aim for durable, drug-free remission. Spontaneous immune control of viremia occurs rarely and with variable permanence. Collins et al. report that selective impairment of HIV-specific CD8$^+$ T cell proliferation and cytolytic capacity precedes aborted control of viremia despite maintained recognition of autologous virus, highlighting key immunologic and virologic parameters of durable HIV control.

Graphical Abstract

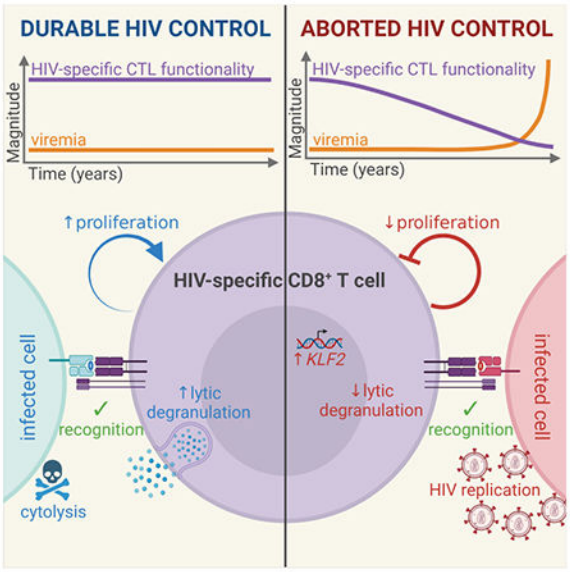

Keywords

Human immunology; HIV control; CD8$^+$ T cell dysfunction

INTRODUCTION

A minority of persons living with human immunodeficiency virus (HIV) infection are able to control viremia without medication to levels at which transmission and disease progression are markedly diminished. Genome-wide association studies in these individuals demonstrated that the major genetic determinants of HIV control affect HLA class I peptide presentation (Pereyra et al., 2010), implying a central role for CD8$^+$ T cell responses. Consistent with this, depletion of CD8$^+$ T cells resulted in loss of viral control in non-human primates (Chowdhury et al., 2015; Friedrich et al., 2007). Moreover, HIV control

has been strongly associated with robust proliferative and cytolytic effector functions of HIV-specific $CD8^+$ T cells (Betts et al., 2006; Hersperger et al., 2010; Migueles et al., 2002; Migueles et al., 2008; Ndhlovu et al., 2013; Saez-Cirion et al., 2007). Recent work revealed that proliferative $CD8^+$ T cell responses in controllers target mutationally constrained HIV epitopes derived from structurally interconnected regions of the viral proteome, irrespective of HLA allele (Gaiha et al., 2019). Thus, HIV controllers provide a blueprint for the development of $CD8^+$T cell-mediated therapeutic and preventive strategies to obviate the need for lifelong adherence to daily antiretroviral therapy (ART) and end the HIV pandemic (Collins et al., 2020; Rogan and Connors, 2021). A deeper understanding of the requirements for durable $CD8^+$ T cell-mediated HIV control will likely be critical to advancing these goals.

Although most HIV controllers maintain durable suppression of viremia for decades, approximately 1-2% lose viral control each year (Yang et al., 2017). In large cohort studies, persistent low-level viremia and history of viral blips were identified as significant risk factors, but were neither necessary nor sufficient for subsequent loss of control, and no additional clinical or demographic parameters were consistently implicated (Borrell et al., 2021; Chereau et al., 2017; Grabar et al., 2017; Leon et al., 2016; Madec et al., 2013; Noel et al., 2015; Yang et al., 2017). Recent studies profiling immune responses in these individuals indicated that loss of HIV control can occur in the absence of superinfection or mutational escape (Koofhethile et al., 2016; Pernas et al., 2018; Rosas-Umbert et al., 2019); however, the mechanisms underlying loss of HIV control remain unclear.

To investigate mechanisms of durable and aborted HIV control, we evaluated antiviral $CD8^+$ T cell specificity, functionality, transcriptional profile and lymphoid tissue localization in individuals who maintain or lose control of viremia. To mitigate against potentially confounding effects of uncontrolled viremia and $CD4^+$ T cell depletion such as those seen in chronic progressors, we focused on longitudinal samples preceding aborted HIV control in which fold changes in $CD4^+$ T cell counts were similar to durable control. Despite maintained recognition of autologous virus, HIV-specific $CD8^+$ T cell proliferative and cytolytic capacities were diminished prior to aborted control in blood and lymphoid tissue, corresponding to increased antiproliferative gene expression and indicating a selective, progressive and intrinsic functional defect that is not revealed by canonical exhaustion or senescence markers.

RESULTS

Subject demographics, genotypes, clinical parameters, circulating biomarkers and proviral reservoirs.

We selected 34 subjects with clade B HIV infections who spontaneously controlled viremia to below 2000 viral RNA copies per ml plasma without ART for a minimum of two years and from whom cryopreserved longitudinal peripheral blood specimens were available. Among this group, 17 subjects maintained durable control and 17 experienced aborted control of viremia, defined by a greater than tenfold increase in viral load to above 2000 copies per ml plasma without a return to stable ART-free viral control (Figures 1A, S1). We focused our analyses on subjects with comparable baseline viremia and with longitudinal

samples preceding aborted control (T1-T3), either before or early during rise in plasma viral loads, in order to identify prognostic indicators and better segregate causal from consequential associations.

Within this cohort, subjects with durable and aborted control were similar in age, sex, race/ethnicity, baseline viral load and $CD4^+$ T cell count, and fold change in $CD4^+$ T cell count over time (Table 1). Protective *HLA-B* alleles (*HLA-B*57*, *B*52*, *B*27*, and *B*14*) defined by genome-wide association in spontaneous HIV controllers (Pereyra et al., 2010) were present at equal frequencies in subjects with aborted and durable control (Table 1). We also assessed circulating proteome, metabolome and lipidome profiles and found no differences between groups (Figure S2A) or longitudinally (Figure S2B) among 209 proteins, 77 metabolites and 115 lipids identified by mass spectrometry-based shotgun multi-omics (Table S1). HIV controllers are known to harbor smaller residual intact proviral reservoirs relative to noncontrollers (Jiang et al., 2020), but both total and intact proviral reservoirs were similar prior to aborted and durable HIV control (Figure S2C-F). These results indicate similarity in clinical, genetic and virologic parameters between these two groups at baseline, providing substantial opportunity to elucidate additional differentiating factors.

HIV-specific $CD8^+$ T cells maintain recognition of autologous HIV during aborted viral control.

Given their prominent role in spontaneous control of HIV viremia (Migueles and Connors, 2015), we next examined proliferative $CD8^+$ T cell responses in subjects with durable or aborted control. To identify functional HIV-specific $CD8^+$ T cell responses, we measured proliferation (Figure 1B) following stimulation with an array of HIV peptides restricted by each subject's class I *HLA* genotype (Table S2). At baseline (T1), neither the number (breadth) nor magnitude of proliferative HIV-specific $CD8^+$ T cell responses (Figure 1C-D) were significantly associated with subsequent loss of viral control.

We next assessed the extent to which mutational escape from $CD8^+$ T cell recognition contributed to aborted control. Proliferative $CD8^+$ T cell responses in aborted and durable control targeted HIV epitopes with similar levels of mutational constraint, as predicted by structure-based network analysis (Gaiha et al., 2019), with the majority of subjects in both groups targeting one or more epitopes predicted to be highly mutationally constrained (Figure 1E). To assess longitudinal mutation within epitopes targeted by autologous $CD8^+$ T cell responses directly, we performed next-generation sequencing of plasma HIV RNA isolated before and after aborted control in ten subjects. Targeted epitope sequences were not mutated over time in 14 of 19 responses with sequence data (Figure 1F), and for the additional 5 responses nonsynonymous epitope sequence variants were detected (Table S3) but only one of the observed variants abrogated recognition by autologous $CD8^+$ T cells collected before aborted control (Figure 1G). Notably, the subject from which this escape variant was detected had two other responses without escape. We also performed phylogenetic analysis of longitudinal plasma HIV sequences, in which sister grouping of paired longitudinal sequences showed no evidence of superinfection (Figure 1H). These results indicate that HIV-specific $CD8^+$T cells maintain recognition of autologous HIV

during aborted viral control, as neither mutational escape nor superinfection were primary mechanisms of aborted HIV control in this cohort.

HIV-specific CD8$^+$ T cell proliferative and cytolytic capacities are progressively, selectively and intrinsically impaired preceding aborted viral control.

Given loss of control despite sustained recognition of antigen, we next assessed changes in T cell phenotype and functionality preceding aborted HIV control. Frequencies of circulating CD8$^+$ and CD4$^+$ T cells were similar over time among subjects with durable and aborted control (Figure S3A), and we observed no significant longitudinal or between-group differences in bulk CD8$^+$ T cell memory subset frequencies as defined by CD45RA and CD62L expression (Figure S3B). HIV-specific CD8$^+$ T cell frequencies measured by peptide-HLA (pHLA) tetramers corresponding to dominant proliferative responses were similar in aborted and durable control at baseline (Figure 2A) and were not significantly changed over time (Figure 2B). Phenotypic staining classified the majority of HIV-specific CD8$^+$ T cells as effector-memory, and their subset composition was maintained longitudinally in both groups (Figure 2C).

To assess longitudinal changes in CD8$^+$ T cell functionality, we measured proliferation of HIV-specific responses upon peptide stimulation at serial time points preceding aborted control. Whereas HIV-specific CD8$^+$ T cell proliferative capacity was maintained over time in subjects with sustained HIV control, it was progressively diminished before loss of control, where 71.4% of responses declined by more than two-fold in proliferative capacity compared with only 8.3% of responses in those who maintained control (Figures 2D and S3C). Despite variability in the abruptness with which control of viremia was lost (Figure S1), reduction in proliferative capacity preceded increases in plasma viral loads in many individuals and was often apparent by time point T2, and the magnitude of functional impairment was not significantly associated with modest increases in viremia prior to aborted control (Figure S3D-E). Notably, this decline in functionality was limited to HIV-specific responses, as CD8$^+$ T cell proliferation upon stimulation with pooled cytomegalovirus (CMV), Epstein-Barr virus (EBV) and influenza A virus (IAV) HLA class-I optimal peptide antigens (Figure 2E) or with anti-CD3 and anti-CD28 agonistic antibodies (Figure 2F) was maintained over time in both groups. Lytic degranulation and production of interferon-γ and tumor necrosis factor-α (but not interleukin-2) upon four-hour antigenic stimulation were also significantly impaired preceding aborted control relative to durable control (Figure S3).

To determine whether impairment of HIV-specific CD8$^+$T cell function preceding aborted control was cell intrinsic or caused in trans by longitudinal changes in other cell types during peptide-specific expansion, we performed proliferation assays by co-culturing CD8$^+$ T cells obtained from early (T1) and late (T3) samples with CD8-depleted, HIV peptide-pulsed peripheral blood mononuclear cells (PBMCs) from either T1 or T3 (Figure 3A). CD8-depleted PBMCs from T1 did not rescue proliferation of HIV-specific CD8$^+$ T cells obtained from T3, and CD8-depleted PBMCs from T3 did not significantly impair proliferation of HIV-specific CD8$^+$ T cells from T1 (Figure 3B). Thus, functional impairment was neither

restored nor recapitulated by interactions with other cell types, suggesting that the defect is $CD8^+$ T cell intrinsic in nature.

We also examined cytolytic capacity of HIV-specific $CD8^+$ T cells prior to aborted control. $CD8^+$ T cells from each longitudinal sample were expanded by stimulation with their dominant HIV response peptide, and then assessed for their ability to eliminate peptide-pulsed autologous $CD4^+$ T cells pooled from all time points in a 6-hour coculture over a range of effector-to-target ratios (Figure 3C). HIV-specific $CD8^+$ T cells exhibited significant longitudinal decline in cytolytic capacity preceding loss of HIV control (Figure 3D), whereas cytolytic responses were maintained in subjects with durable control. Taken together, these results provide evidence that HIV-specific $CD8^+$ T cell proliferative and cytolytic capacities are progressively, selectively and intrinsically impaired preceding aborted viral control.

Transcriptomes but not TCR repertoires of HIV-specific $CD8^+$ T cells are altered preceding aborted viral control.

Having identified functional impairment of HIV-specific $CD8^+$ T cells preceding loss of viral control, we next sought to define underlying molecular signatures using whole-transcriptome RNA sequencing of immunodominant pHLA $tetramer^+$ $CD8^+$ T cell populations isolated from longitudinal specimens in both groups. We detected a mean of 16,510 unique genes per sample (Figure 4A) and analyzed differential expression across 18,091 genes. We observed 530 significantly differentially expressed genes prior to loss or maintenance of control (Figure 4B, Table S4). Of these, 471 genes were not significantly differentially expressed at baseline (Figure 4C) and therefore correspond to differences observed in proliferative and cytolytic capacity.

Gene set enrichment analysis revealed that aborted control was preceded by increased expression of genes related to GTPase activity, transcriptional repression and G2/M cell cycle arrest, and also by decreased expression of genes related to cytokine-mediated signaling, T cell activation and degranulation (Figure 4D, Table S5). Notably, the transcription factor *KLF2*, which limits $CD8^+$ T cell proliferation (Buckley et al., 2001), was among the most significantly elevated genes prior to loss of HIV control (Figure 4E), representing a candidate transcriptional regulator of $CD8^+$ T cell functional impairment in these individuals. KLF2 is also known to regulate T cell trafficking, differentiation and effector function (Lee et al., 2015; Preston et al., 2013; Weber et al., 2015). To further characterize KLF2 regulation of HIV-specific $CD8^+$ T cell transcription preceding aborted control, we performed single-sample gene set enrichment analyses (ssGSEA) on known KLF2-regulated genes and pathways. KLF2-regulated effector, cytokine and chemokine receptor genes were significantly downregulated prior to aborted control (Figure S5), consistent with a potential role of KLF2 in decreased HIV-specific $CD8^+$ T cell functionality preceding aborted viral control.

We also determined the extent to which functional changes in HIV-specific $CD8^+$ T cells were associated with longitudinal changes in TCR clonotype composition, since $CD8^+$ T cell signaling and functionality are dictated in part by molecular interactions between TCR and pHLA, and the specificity, cross-reactivity, affinity, geometry and kinetics of these

interactions are determined by the repertoire of TCR sequences within polyclonal antigen-specific T cell populations (Rossjohn et al., 2015). We analyzed a mean of 10,949 TCR-β (*TRB*) complementarity determining region 3 (CDR3) sequence reads per sample within whole-transcriptome RNA-seq data from HIV-specific $CD8^+$ T cells, which were generally oligoclonal with relatively few clonotypes per response. Only 1 of 5 subjects analyzed from each group exhibited a longitudinal shift in the dominant TCR clonotype preceding loss or maintenance of viral control, whereas the remaining 8 subjects maintained consistent TCR clonotypic compositions over time (Figure S6), and longitudinal shifts in TCR clonotypic diversity were not significantly associated with loss of HIV control (Figure 4F). These results provide additional evidence that changes in HIV-specific $CD8^+$ T cell transcription and functionality but not antigenic recognition precede aborted control in our cohort.

Functional impairment preceding aborted HIV control is distinct from T cell exhaustion and senescence.

$CD8^+$ T cell dysfunction has been extensively described in settings of prolonged antigen exposure, including HIV infection and cancer, and is commonly associated with increased expression of inhibitory receptors and other markers of T cell exhaustion and senescence during chronic uncontrolled viremia (Fenwick et al., 2019; McLane et al., 2019). Using ssGSEA, we next examined expression of a core set of 20 exhaustion-associated genes, including 10 inhibitory receptors and 10 transcriptional regulators that were significantly upregulated in $CD8^+$ T cells during chronic LCMV infection (Figure S7A), uncontrolled chronic HIV infection (Figure S7B) and melanoma tumor infiltration (Figure S7C). However, within our RNA-seq data set we did not observe significant differential expression of this core exhaustion gene set in HIV-specific $CD8^+$ T cells with diminished functionality prior to aborted viral control (Figure 5A). We also measured surface expression of the exhaustion-associated inhibitory receptors PD1, TIM3, TIGIT, CD39, 2B4 and CD160, the senescence-associated surface marker CD57 and the costimulatory receptor CD28. Surface expression for each of these proteins was not significantly perturbed across longitudinal samples on HIV-specific $CD8^+$ T cells (Figure 5B-I), despite reductions in proliferative and cytolytic capacity of these cells. Together, these data indicate that progressive loss of $CD8^+$ T cell function preceding aborted control is transcriptionally and phenotypically distinct from canonical exhaustion or senescence.

Lymphoid HIV-specific $CD8^+$ T cells are functionally impaired during aborted viral control.

Follicular helper $CD4^+$ T cells in lymphoid tissue represent a major source of HIV replication and comprise a significant proportion of persistent viral reservoirs in both HIV controllers and ART-suppressed progressors (Boritz et al., 2016; Perreau et al., 2013), highlighting the importance of studying HIV immune dynamics at tissue sites of infection in addition to peripheral circulation. Expanding our analyses to tissues, we obtained one inguinal lymph node per group via excisional biopsy during either durable or aborted control. To qualitatively determine the extent to which $CD8^+$ T cells can access HIV-infected cells in lymphoid follicles, we performed *in situ* fluorescence microscopy for CD8, immunoglobulin D (IgD) to demarcate lymphoid follicles and HIV *gagpol* RNA to mark HIV-infected cells. During durable control we observed clear follicular margins with intrafollicular HIV-infected cells and primarily extrafollicular $CD8^+$ cells (Figure 6A),

consistent with reports that lymphoid follicles largely exclude $CD8^+$ T cells and contain viral replication within follicular sanctuaries (Connick et al., 2014; Connick et al., 2007; Fukazawa et al., 2015). In contrast, during aborted control we observed disrupted follicular margins, likely resulting from viral replication, and the presence of $CD8^+$ T cells in close proximity to HIV-infected cells (Figure 6B).

To assess the functionality of lymphoid HIV-specific $CD8^+$ T cells, we performed proliferation and elimination assays using cells isolated from matched peripheral blood (PB) and lymph node (LN) specimens. Relative to durable control, we observed that both PB and LN HIV-specific $CD8^+$ T cells during aborted control were markedly less proliferative in response to antigenic stimulation (Figure 6C). Following antigen-specific expansion, both lymphoid and peripheral HIV-specific $CD8^+$ T cells exhibited poor elimination of autologous HIV peptide-loaded $CD4^+$ T cells during aborted control relative to durable control (Figure 6D). These results indicate that virus-specific $CD8^+$ T cells can access lymphoid follicles during aborted control but are functionally impaired, consistent with observations made from peripheral blood.

DISCUSSION

In this study, we examined immunologic and virologic parameters longitudinally in individuals who spontaneously controlled HIV viremia to distinguish mechanisms of durable and aborted viral control. Compared to durable control, aborted control was preceded by a progressive decline in HIV-specific $CD8^+$ T cell proliferative and cytolytic function without mutational escape from antigen recognition. This loss of function was T cell intrinsic, restricted to HIV-specific responses, and evident in both peripheral blood and lymphoid tissue. Functional impairment of HIV-specific $CD8^+$ T cells was accompanied by decreased expression of genes related to activation and cytokine-mediated signaling, and increased expression of the antiproliferative transcription factor *KLF2*. In contrast, expression of genes and surface inhibitory receptors associated with canonical T cell exhaustion or senescence were not elevated. Collectively, these findings identify alterations in virus-specific T cell function that portend loss of HIV control in a manner transcriptionally and phenotypically distinct from canonical T cell exhaustion.

Prior studies of $CD8^+$ T cell function during aborted HIV control primarily focused on cytokine responses to pooled antigen and activation/exhaustion marker expression in bulk $CD8^+$ T cells. To extend beyond this, we studied antigen-specific responses in subjects from whom specimens had been obtained longitudinally prior to aborted or durable control, allowing a detailed analysis of virologic and immunologic parameters that predict subsequent loss of control. Marked longitudinal decreases in proliferative and cytolytic capacities of HIV-specific $CD8^+$ T cells preceding aborted control reported here are consistent with reduced polyfunctionality and reduced virus suppression shown among polyclonal $CD8^+$ T cell responses in other cohorts (Koofhethile et al., 2016; Pernas et al., 2018; Rosas-Umbert et al., 2019).

Previous cross-sectional studies have shown that spontaneous control of viremia is associated with proliferative HIV-specific $CD8^+$ T cell responses, cytolytic capacity and

polyfunctionality (Betts et al., 2006; Hersperger et al., 2010; Migueles et al., 2002; Migueles et al., 2008; Migueles et al., 2020; Ndhlovu et al., 2013; Saez-Cirion et al., 2007). Recent work has further elucidated mechanisms by which the ability of HIV-specific $CD8^+$ T cells to expand and generate secondary effector cells is regulated in elite HIV controllers (Rutishauser et al., 2021; Sekine et al., 2020). Conversely, functional defects in HIV progressors have largely been attributed to T cell exhaustion, senescence and necroptosis associated with chronic uncontrolled viremia (Day et al., 2006; Gaiha et al., 2014; Papagno et al., 2004; Petrovas et al., 2006; Trautmann et al., 2006). Although we observed modest but significant increases in plasma viral load over time before aborted control in some individuals, these were neither significantly associated with the magnitude of functional impairment observed nor with transcript or surface expression of exhaustion or senescence markers on dysfunctional HIV-specific cells. Importantly, although inhibitory receptor expression is upregulated upon T cell activation during uncontrolled viremia (Ahn et al., 2018) it becomes reduced to levels comparable with elite controllers during suppressive ART despite continued dysfunction of HIV-specific responses (Migueles et al., 2009), raising the possibility that functional impairment during aborted control and treated chronic infection may share common mechanisms that warrant further investigation.

In order to elucidate molecular mechanisms by which HIV-specific $CD8^+$ T cells become functionally impaired preceding aborted viral control, we performed whole-transcriptome RNA-seq of antigen-specific $CD8^+$ T cells. This revealed alterations in gene expression associated with reduced cytokine-mediated signaling, T cell activation and degranulation, and increased GTPase signaling, cell cycle regulation and transcriptional repression preceding aborted control. The transcription factor *KLF2* was among the most significantly upregulated genes prior to aborted HIV control, representing a candidate regulator of functional impairment in these cells. *KLF2* was previously shown to regulate T cell quiescence (Kuo et al., 1997) and long-term survival of resting memory $CD8^+$ T cells (Schober et al., 1999), in addition to its role in T cell trafficking (Bai et al., 2007). *KLF2* overexpression in T cells impaired proliferation whereas *KLF2* silencing induced spontaneous cell cycling (Buckley et al., 2001), demonstrating that *KLF2* limits T cell proliferation. *KLF2* is also downregulated upon TCR signaling (Preston et al., 2013), so it is possible that the relative increase in expression prior to aborted versus durable HIV control may reflect a defect in T cell activation. Consistent with this, gene sets associated with T cell activation, effector function and cytokine production were decreased in individuals losing control of HIV despite increasing antigenemia, suggesting a potential defect in the ability of HIV-specific $CD8^+$ T cells to activate in vivo. These findings provide insights into the transcriptional regulation of durable and aborted HIV control and further support a model in which the ability of HIV-specific memory $CD8^+$ T cells to robustly activate and expand is essential for maintenance of cytolytic potential, likely through generation of secondary effectors, whereas loss of proliferative capacity leads to the inability to maintain cytolytic control of viral replication.

While most studies of immune function have been limited to peripheral blood due to ease of access, immunity within tissue sites of infection has recently come into greater focus. Lymphoid tissues are especially relevant for HIV infection as they harbor large viral reservoirs within follicular helper $CD4^+$ T cell-rich follicles (Boritz et al., 2016; Estes et al.,

2017; Perreau et al., 2013). CXCR5$^+$ follicular CD8$^+$ T cells that can enter these regions have been associated with control and containment of viral replication (Connick et al., 2014; He et al., 2016; Leong et al., 2016), and expression of follicular homing receptors is partially controlled by KLF2 (Lee et al., 2015; Weber et al., 2015). Lymphoid HIV-specific CD8$^+$ T cells exhibit tightly regulated expression of cytolytic effector molecules, with low levels of expression at steady state in the absence of antigen within elite controller lymph nodes (Buggert et al., 2018; Nguyen et al., 2019; Reuter et al., 2017). Using different methodology, our findings reveal that although CD8$^+$ T cells were observed proximal to follicular HIV replication, their capacity for expansion and acquisition of cytolytic function in response to antigen distinguished durable from aborted control.

In addition to changes preceding aborted control, we also identified many parameters that remained comparatively unchanged. Neither baseline plasma viremia nor total or intact HIV reservoir size was associated with loss or maintenance of HIV control in our cohort. Moreover, while proteomic and metabolomic analyses identified candidate biomarkers associated with loss of HIV control in another cohort (Rodriguez-Gallego et al., 2019; Tarancon-Diez et al., 2019), no significant changes in plasma proteomes, metabolomes or lipidomes were detectable during loss of HIV control in our cohort using a similar approach, indicating that soluble circulating biomarkers may not reliably predict loss of control across cohorts with different clinical and demographic characteristics. Mutational escape from CD8$^+$ T cell recognition, which has been observed in acute (Allen et al., 2005) and chronic HIV infection (Goulder et al., 1997), was infrequent preceding loss of control, consistent with other recent studies showing relatively low mutational frequency during loss of HIV control (Koofhethile et al., 2016; Rosas-Umbert et al., 2019) and with studies reporting that HIV control often persists despite epitope mutations via de novo or cross-reactive T cell responses (Bailey et al., 2006; Chan et al., 2020; Miura et al., 2009; Pohlmeyer et al., 2013). Superinfection, which can also drive immune escape (Altfeld et al., 2002), was not observed among subjects with aborted control in our cohort and was also rare among others (Pernas et al., 2018; Rosas-Umbert et al., 2019). Furthermore, we show that TCR clonotypic composition of HIV-specific CD8$^+$ T cell responses was maintained over time, consistent with maintained recognition of cognate antigen. Taken together, these findings demonstrate that impaired CD8$^+$ T cell functionality rather than escape from immune surveillance is the predominant mechanism for loss of viral control.

In summary, we provide evidence that loss of HIV control occurs following selective loss of virus-specific CD8$^+$ T cell effector functions in blood and lymphoid tissue via a mechanism that is transcriptionally and phenotypically distinct from canonical exhaustion or senescence, further demonstrating that maintenance of HIV-specific CD8$^+$ T cell functionality is a key component of durable control of viremia. This work has implications for immune monitoring of spontaneous controllers and development of immunotherapies to achieve durable CD8$^+$ T cell-mediated HIV remission.

Limitations of the study

Cohort size and demographic composition were limited by availability of longitudinal specimens meeting the study criteria. Cryopreserved samples from available time points

were limited, and therefore we focused on defined HLA-optimal epitopes and clade B consensus sequence peptides, potentially missing additional responses to autologous virus. Limited cell numbers also prevented deeper characterization of molecular mechanisms of HIV-specific $CD8^+$ T cell functional impairment, including epigenetic and single-cell assays. Results in which modest differences failed to reach statistical significance may have also been limited by sample size. Cryopreservation of samples may have altered cellular phenotypes. Access to tissue specimens was particularly limited, and longitudinal sampling of lymphoid tissue was unavailable. Importantly, our study was unable to pinpoint specific triggers that initiated loss of HIV-specific $CD8^+$ T cell functionality in vivo. Such events may have preceded sampling in our study and/or may involve events in tissue sites of infection not readily detectable in peripheral blood. While our study did not identify plasma biomarkers to predict loss of control, the data provide insight into transcriptional and functional changes that may inform monitoring of HIV controllers for risk of impending virologic disease progression. Although we did not observe phenotypic evidence of canonical T cell exhaustion, we did observe its functional hallmarks, possibly indicating an orthogonal dysfunction pathway or an earlier stage in the same pathway. We identified altered transcriptional programs distinct from canonical T cell exhaustion and a candidate transcriptional regulator; however, further investigation into precise molecular mechanisms of HIV-specific $CD8^+$ T cell dysfunction, mechanistic similarities in broader populations of people living with HIV, and the extent to which functionality can be restored remain as important future directions.

STAR METHODS

Resource availability

Lead contact—Further information and requests for resources and reagents should be directed to and will be fulfilled by the Lead Contact, Bruce D. Walker (bwalker@mgh.harvard.edu).

Materials availability—This study did not generate new unique reagents.

Data and code availability

- RNA-seq data have been deposited at GEO and are publicly available as of the date of publication. Plasma viral sequencing data have been deposited in Genbank and are publicly available as of the date of publication. Accession numbers are listed in the key resources table. Due to subject confidentiality concerns, full-length proviral sequencing data cannot be deposited in a public repository but will be made available to investigators upon reasonable request with an appropriate data use agreement. This paper analyzes existing, publicly available data. These accession numbers are listed in the key resources table.
- This paper does not report original code.
- Any additional information required to reanalyze the data reported in this paper is available from the lead contact upon request.

Experimental model and subject details

Human subjects—Peripheral blood and excisional inguinal lymph node biopsy samples were collected from HIV controllers with written informed consent after study approval by the Institutional Review Board of Massachusetts General Hospital (Boston, MA). Viral load and complete blood count records were obtained from healthcare providers with subject consent. Aborted control (AC) was defined as individuals with three or more years of documented HIV control to viral loads below 2000 copies/mL in absence of ART prior to a 1-log or greater viral load increase to above 2000 copies/mL without subsequent return to stable control (due to continued viral load increase and/or ART initiation). Durable control (DC) was defined by maintenance of viral loads below 2000 copies/ml. Demographic and clinical characteristics are reported in Table 1 and Figure S1.

Method details

Specimen processing—Longitudinal specimens were obtained for multiple sample time points preceding (T1-T3) and following (T4) aborted control of viremia. Plasma and density gradient isolated PBMCs were cryopreserved in liquid nitrogen. *HLA* genotyping was performed by Dr. Mary Carrington (National Cancer Institute, Bethesda, MD). Inguinal lymph node biopsy tissue was obtained surgically with informed consent and was processed into both formalin-fixed paraffin-embedded sections for microscopy and mononuclear cell suspensions for cellular assays. Frozen cells were thawed at 37°C and recovered in RPMI supplemented with 10% fetal bovine serum (FBS, Sigma) overnight prior to functional and phenotypic assays.

Plasma multi-omics—Serum proteomics, lipidomics and metabolomics were performed by staff from Proteomics and Metabolomics facilities of the Centre for Omic Sciences (COS) Joint Unit of the Universitat Rovira I Virgili-Eurecat. Longitudinal plasma samples from 11 subjects with AC and 9 with DC spanning 2-3 time points before and 1 time point after AC were analyzed as follows:

For proteomic analysis, depletion of the seven most abundant plasma proteins (Albumin, IgG, antitrypsin, IgA, transferrin, haptoglobin and fibrinogen) was performed in order to increase the number of identified/quantified proteins. Thus, 12 µl of each sample were passed twice through the Human-7 Multiple Affinity Removal Spin (MARS) cartridge (Agilent) and flow-through fractions were collected for proteomic analysis. Flow-through fractions were concentrated and buffer exchanged to about 100 µl of 6M urea in 50 mM ammonium bicarbonate (ABC) by using 5K MWCO spin columns (Agilent). 30 µg of total protein (quantified by Bradford's method, see Table 3 on results section) were reduced with 4 mM 1.4-Dithiothreitol (DTT) for 1h at 37°C and alkylated with 8 mM iodoacetamide (IAA) for 30 min at 25°C in the dark. Afterwards, samples were overnight digested (pH 8.0, 37°C) with sequencing-grade Trypsin/Lys-C Protease Mix (Thermo Fisher) at enzyme:protein ratio of 1:50. Digestion was quenched by acidification with 1% (v/v) formic acid and peptides were desalted on Oasis HLB SPE column (Waters) before TMT 11-plex labelling (Thermo Fisher) following manufacturer instructions. To normalize all samples in the study along the different TMT-multiplexed batches used, a pool containing all the samples was labelled with TMT-126 tag and included in each TMT batch. The different

TMT 11-plex batches were desalted on Oasis HLB SPE columns before the nanoLC-MS analysis. Labelled and multiplexed peptides were loaded on a trap nano-column (100 μm I.D.; 2cm length; 5μm particle diameter, Thermo Fisher) and separated onto a C-18 reversed phase (RP) nano-column (75μm I.D.; 15cm length; 3μm particle diameter, Nikkyo Technos) on an EASY-II nanoLC (Thermo Fisher). The chromatographic separation was performed with a 180 min gradient using Milli-Q water (0.1% formic acid) and acetonitrile (0.1% formic acid) as mobile phase at a flow rate of 300 nL/min. Each TMT-plex was analyzed in triplicate in order to increase peptide and protein coverage. Mass spectrometry analyses were performed on an LTQ-Orbitrap Velos Pro (Thermo Fisher) by an enhanced FT-resolution MS spectrum (R=30,000 FHMW) followed by a data dependent FT-MS/MS acquisition (R=15,000 FHMW, 40% HCD) from the most intense ten parent ions with a charge state rejection of one and dynamic exclusion of 0.5 min. Protein identification/ quantification was performed on Proteome Discoverer software v.1.4.0.288 (Thermo Fisher) by Multidimensional Protein Identification Technology (MudPIT) combining the 3 raw data files obtained from each sample. For protein identification, all MS and MS/MS spectra were analyzed using Mascot search engine (v.2.5). The workflow was set up using two different Mascot node combing Homo Sapiens database (74449 entries) and contaminants database (247 entries), both searches assuming trypsin digestion. Two missed cleavages were allowed and an error of 0.02 Da for FT-MS/MS fragmentation mass and 10.0 ppm for a FT-MS parent ion mass were allowed. TMT-10plex was set as quantification modification and oxidation of methionine and acetylation of N-termini were set as dynamic modifications, whereas carbamidomethylation of cysteine was set as static modifications. The false discovery rate (FDR) and protein probabilities were calculated by Percolator (Kall et al., 2007). For protein quantification, the ratios between each TMT-label against 126-TMT label were used and quantification results were normalized based on protein median. The results are a ratio of reporter ions abundance and are dimensionless.

For lipidomic analysis, extraction of hydrophobic lipids was performed by liquid-liquid extraction with chloroform:methanol (2:1) based on Folch procedure was performed by adding four volumes of chloroform:methanol (2:1) containing SPLASH Lipidomix internal standard mixture (Sigma) to serum. Samples were then mixed and incubated at −20°C for 30 min. Afterwards, water with NaCl (0.8 %) was added and mixture was centrifuged at 15,000 rpm. Lower phase was recovered, evaporated to dryness and reconstituted with methanol:methyl-tert-butyl ether (9:1) and analyzed by UHPLC-qTOF 6550 (Agilent) in positive electrospray ionization mode. The chromatographic consist in an elution with a ternary mobile phase containing water, methanol and 2-propanol with 10mM ammonium formate and 0.1% formic acid. The stationary phase was an EVO C18 column (Kinetex) allowing sequential elution of hydrophobic lipids. Identification of lipid species was performed by matching their accurate mass and tandem mass spectrum, when available, to Metlin-PCDL (Agilent) containing more than 40,000 metabolites and lipids. In addition, chromatographic behavior of pure standards for each family and bibliographic information was used to ensure their putative identification. After putative identification of lipids, these were semi quantified in terms of internal standard response ratio using one internal standard for each lipid family.

For metabolomic analysis, a protein precipitation extraction was performed by adding eight volumes of methanol:water (8:2) containing internal standard mixture (succinic acid-d4, myristic acid-d27, glicerol-13C3 and D-glucose-13C6) to serum samples. Then, the samples were mixed and incubated at 4°C for 10 min., centrifuged at 15,000 rpm and supernatant was evaporated to dryness before compound derivatization (metoximation and silylation). The derivatized compounds were analyzed by GC-qTOF 7200 (Agilent). The chromatographic separation was based on Fiehn Method, using a HP5-MS 0.25 μm film capillary column (J&W Scientific) and helium as carrier gas using an oven program from 60 to 325°C. Ionization was done by electronic impact (El), with electron energy of 70eV and operated in full Scan mode. In addition to targeted compounds from central carbon metabolism which were quantified using internal standard calibration curves. Citric acid was not quantified since the samples are plasma citrate which invalidates their quantification. A screening for the identification of more metabolites was performed by matching their El mass spectrum and retention time to metabolomic Fiehn library (Agilent) which contains more than 1400 metabolites. After putative identification of metabolites, these were semi-quantified in terms of internal standard response ratio.

Plasma multi-omics results were log base-2 transformed, modeled for subject metadata and analyzed for differences between subject types and longitudinally during AC using limma (Ritchie et al., 2015) for combined proteomics, metabolomics, lipidomics data sets.

Peptide-HLA tetramer and surface staining—Peptide-HLA monomers were obtained from ImmunAware (Copenhagen, Denmark) with the exceptions of A*11:01-ACQGVGGPSHK (Dr. Masafumi Takiguchi, Kumamoto University, Japan) and A*26:01-EVIPMFSAL (MBL International). Tetramers were produced by multimerization with APC-conjugated streptavidin (Biolegend) as per manufacturer's protocol and stored at 4°C for a maximum of 4 weeks prior to use. Staining was performed using individual pH LA tetramers at 4°C prior to surface marker staining to prevent cell activation and steric interference. Where indicated, cells were also stained with BUV395-conjugated anti-CD8 (clone RPA-T8, BD Biosciences), APC/Cy7-conjugated anti-CD45RA (clone HI100, Biolegend) and FITC-conjugated anti-CD62L (clone DREG-56, Biolegend) and Live/Dead Violet viability dye (Thermo Fisher); or with BUV395-conjugated anti-CD8 (clone RPA-T8, BD Biosciences), BV605-conjugated anti-PD1 (clone EH12.2H7, Biolegend), AlexaFluor 488-conjugated anti-TIM3 (clone 344823, R&D Systems), PE/Dazzle 594-conjugated anti-TIGIT (clone A15153G, Biolegend), PE/Cy7-conjugated anti-CD160 (clone BY55, Biolegend), PerCP/Cy5.5-conjugated anti-2B4 (clone C1.7, Biolegend), BV650-conjugated anti-CD39 (clone TU66, BD Biosciences), BV510-conjugated anti-CD57 (clone HNK-1, Biolegend) and APC/Cy7-conjugated anti-CD28 (clone CD28.2, Biolegend) and analyzed by flow cytometry.

Flow cytometry and FACS—Flow cytometry and cell sorting were performed at the Ragon Institute flow cytometry and imaging core using BD Fortessa and LSR-II cytometers, FACSAria sorters and FACSDiva software (Becton Dickinson). Flow cytometric analyses were performed using FlowJo v10.0.8 (TreeStar).

Proliferation assay—$CD8^+$ T cell proliferation was assessed both for response screening and quantitation as previously described (Gaiha et al., 2019). Briefly, mononuclear cells were stained at 37°C for 20 minutes with 0.5 μM CellTrace carboxyfluorescein succinimidyl ester (CFSE; Thermo Fisher) as per manufacturer's protocol at $1x10^6$ cells/mL. Staining was quenched with FBS (Sigma), cells were washed twice with RPMI supplemented with 10% FBS (R10), resuspended at $1x10^6$/mL and plated 200 μL per well in 96-well round-bottom polystyrene plates (Corning). Individual HLA-optimal HIV peptides matched to each subject's *HLA* genotype (see Table S2), selected from Los Alamos National Laboratory's "A-list" of HLA-optimal HIV-1 epitopes (Llano et al., 2019), were added at 1 μM and incubated at 37°C for 6 days before flow cytometric assessment. Negative control wells did not receive peptide and positive control wells received 1 μg/mL anti-CD3 (clone OKT3, Biolegend) and anti-CD28 (clone CD28.8, Biolegend) antibodies. Where indicated, cells were instead stimulated with pooled CMV, EBV and IAV peptides (Mabtech). On day 6, cells were stained for viability using Live/Dead Violet (Thermo Fisher), AlexaFluor 700-conjugated anti-CD3 (clone SK7, Biolegend), BUV395-conjugated anti-CD8 (clone RPA-T8, BD Biosciences), and where indicated, APC-conjugated pHLA tetramers, then analyzed by flow cytometry. Responses at least 2.5-fold above background were scored as positive. For co-culture proliferation assay experiments, $CD8^-$ cells were isolated by collecting the flowthrough from EasySep Human CD8 Positive Selection Kit II (StemCell Technologies) and $CD8^+$ T cells were separately isolated from PBMCs via EasySep Human $CD8^+$ T Cell Isolation Kit (StemCell Technologies). $CD8^+$ T cells and $CD8^-$ cells were cocultured at a 1:5 ratio approximating their natural frequencies in PBMCs, including cocultures from the same time point and across time points from autologous subjects in the proliferation assay described above.

Viral sequencing—HIV RNA was isolated from plasma after ultracentrifugation using the Qiaamp Viral RNA Mini kit (Qiagen). *Gag, pol*, and 3' half or *Nef* amplicons were amplified by nested RT-PCR and sequenced on MiSeq (Illumina), as described previously (Tully et al., 2016). Paired reads were assembled into consensus sequences using Vicuna (Yang et al., 2012), annotated using V-FAT and aligned to consensus using Mosaik (Lee et al., 2014). Variants were called using V-Phaser 2 (Yang et al., 2013) and Vprofiler was used to determine haplotype sequences and calculate epitope mutational frequencies (Henn et al., 2012). Phylogenetic analysis was performed using SeaView (Gouy et al., 2010) to assess superinfection; briefly, consensus HIV sequences assembled from plasma sequencing data were aligned using muscle v3.8.31 (Edgar, 2004) and a maximum likelihood tree was generated using PhyML v3.0 (Guindon et al., 2010) with 1000 bootstraps. Reference HIV sequences were included, with clade C consensus as a putative outgroup. Full-length integrated proviral sequencing and quantification of total and intact reservoir sizes were performed as described previously (Jiang et al., 2020; Lee et al., 2017). Briefly, genomic DNA was extracted from PBMC and diluted to single genome quantities as measured by droplet digital PCR (ddPCR). Diluted DNA was subjected to HIV-1 near full-genome amplification via nested PCR. Near-full-length sequences (>8,000 bp) were sequenced via Illumina MiSeq. Reads were de novo assembled and aligned to HXB2 to identify mutations, including 5'-defects, large deletions, hypermutation, premature stop codons and internal inversions. Viral sequences lacking such mutations were considered genome-intact. HIV

epitope network z-scores were calculated previously via structure-based network analysis (Gaiha et al., 2019).

Variant recognition assay—PBMCs collected prior to AC were stimulated for 4 hours with 1 μM of HLA-optimal peptides of clade B HIV consensus and autologous sequences observed in plasma before and after loss of viral control. BV711-conjugated anti-CD107A (clone H4A3, Biolegend) was included during stimulation to measure degranulation. GolgiStop and GolgiPlug (BD Biosciences) were added 2 hours post-stimulation to enable intracellular cytokine staining. Cells were stained with Live/Dead Violet, BV605-conjugated anti-CD3 (clone SK7, Biolegend) and BUV395-conjugated anti-CD8 (clone RPA-T8, BD Biosciences), fixed and permeabilized using Cytofix/Cytoperm (BD Biosciences), stained for intracellular PE/Cy7-conjugated anti-IFN-γ (clone B27, Biolegend) and analyzed via flow cytometry. Recognition was considered maintained if the frequency of $CD107A^+$ IFN-γ^+ $CD8^+$T cells upon variant peptide stimulation was greater than 50% that of baseline autologous peptide stimulation.

Lytic degranulation and intracellular cytokine staining—$CD8^+$ T cells were isolated from peripheral blood via EasySep Human $CD8^+$ T Cell Isolation Kit (StemCell Technologies) and stimulated with 50 nM pH LA tetramer at 37°C for 4 hours in the presence of BV711-conjugated anti-CD107A (clone H4A3, Biolegend) to stain for transient surface expression during cellular degranulation. GolgiStop and GolgiPlug (BD Biosciences) were added after 2 hours to block cytokine secretion. Unstimulated cells were instead stained with pHLA tetramer at 4°C for 15 minutes before surface staining. Cells were stained with BUV395-conjugated anti-CD8 (clone RPA-T8, BD Biosciences) and Live/Dead Violet before fixation and permeabilization with Cytofix/Cytoperm (BD Biosciences) followed by staining with intracellular PE/Cy7-conjugated anti-IFN-γ (clone B27, Biolegend), PerCP/Cy5.5-conjugated anti-TNF-α (clone Mab11, Biolegend), PE-conjugated anti-Perforin (clone B-D48, Biolegend), PE/CF594 anti-granzyme B (clone GB11, BD Biosciences), and BV605-conjugated anti-IL-2 (clone MQ1-17H12, Biolegend) for flow cytometry. Lytic degranulation was calculated as the frequency of $CD107A^+$ $Perforin^+$ Granzyme B^+ cells within the viable pHLA $tetramer^+$ $CD8^+$ T cell population. Gating was established using fluorescence-minus-one controls for pHLA tetramer, CD107A, perforin and granzyme B or using unstimulated controls for IFN-γ, TNF-α and IL-2.

Elimination assay—Elimination assays were performed as previously described (Clayton et al., 2018) with modifications. Mononuclear cells were incubated with individual HLA-optimal HIV peptide for six days to expand antigen-specific responses as described above. Target $CD4^+$ T cells were isolated from PBMC by magnetic isolation (EasySep human $CD4^+$ T cell isolation kit, StemCell Technologies), activated in 2 mg/mL anti-CD3 (clone OKT3, Biolegend) coated 24-well non-treated polystyrene plates (Corning) at 2 million cells/mL in R10 with 2 mg/mL anti-CD28 (clone CD28.2, Biolegend) and 50 U/mL IL-2 (Peprotech) at 37 C overnight, then expanded in treated 24-well plates (Corning) at 2 million cells/mL in R10 with 50 U/mL IL-2 at 37 C for five days. 50% of target cells were pulsed for 30 minutes at 37 C with 1 μM peptide and labeled with CellTrace Far Red dye (Thermo Fisher) and mixed with unpulsed target cells 1:1, then labeled with CellTrace Violet dye

(Thermo Fisher). After six days of expansion, CFSE-labeled effector $CD8^+$ T cells were isolated from pooled mononuclear cells by magnetic isolation (EasySep human $CD8^+$ T cell isolation kit, StemCell Technologies) and co-cultured with target cells at effector:target (E:T) ratios of 0, 1, 2, 4, and 8 with 50,000 target cells/well in a treated 96-well polystyrene plate (Corning) for 6 hours. Effector-only populations were stained with APC-conjugated pHLA tetramers and all samples were stained with BV605-conjugated anti-CD3 (clone SK7, Biolegend), BUV395-conjugated anti-CD8 (clone RPA-T8, BD Biosciences), BV711-conjugated anti-CD4 (clone RPA-T4, Biolegend) and Live/Dead Near-IR (Thermo Fisher) then analyzed by flow cytometry. Elimination results were gated on residual peptide pulsed cells (scatter-intact, singlet, Live/Dead Near-IR^-, $CD8^-$, $CFSE^-$, $CD4^+$, CellTrace $Violet^+$, CellTrace Far Red^+) as a frequency of total CellTrace $Violet^+$ $CD4^+$ target cells. Percent elimination was calculated as shown in Figure 3C and area under curve for varying E:T ratios was calculated using Excel (Microsoft).

Whole-transcriptome RNA and TCR sequencing—Five subjects each with aborted or durable control were selected for analysis on the basis of specimen and $pHLA^+$ tetramer availability. Replicate populations of 1000-5000 HIV-specific $CD8^+$ T cells were sorted by FACS on the basis of staining with individual pH LA tetramers into RLT Plus lysis buffer then frozen at −80 C. RNA was isolated from lysates after thawing on ice and vortex homogenization using AllPrep isolation kit (Qiagen). Whole transcriptome amplification was performed by SmartSeq2 as described (Villani and Shekhar, 2017), tagmented using Nextera XT (Illumina) and sequenced on NextSeq 550 (Illumina) using 75 base paired end reads. Reads were quality controlled using FastQC and aligned to the hg38 reference human transcriptome with bowtie1 using the RSEM pipeline (Li and Dewey, 2011). Genes with fewer than 5 reads in fewer than 10% of samples were excluded from analysis, and samples with fewer than 2000 unique genes with 5 or more reads were also excluded from downstream analyses. Linear models for measuring differential gene expression were developed using forward selection and optimized using AIC and FDR with filtering for collinear terms. Models included terms for biological effects of interest like time point, treatment, subject and subject type, as well as subject metadata and sample quality metrics so as to isolate biological effects of interest and account for potentially confounding subject-specific or QC effects. Differential expression analysis was performed using DESeq2 version 1.26.0 R package (Love et al., 2014). Gene set enrichment analyses were performed using CERNO (Zyla et al., 2019) ranked by FDR-adjusted q values (signed by direction of fold change) with GO:BP, GO:CC, GO:MF, Reactome, Kegg and Hallmark gene sets from MSigDB (Liberzon et al., 2011). Significantly enriched gene sets were organized into directional nearest-neighbor networks using Fisher's tests to quantify overlap between gene sets. Significantly overlapping gene sets below a maximum $\log(p)$ of −90 were grouped into subnets of closely related gene signatures and subnet names were selected to provide a descriptive summary of member gene sets. Violin plots were produced using variance stabilizing transformation of normalized gene counts as described previously (Wang and Fingert, 2012). Single-sample gene set enrichment analysis (ssGSEA, implememnted in the GSVA R package version 1.34.0) (Hanzelmann et al., 2013) was performed for a set of twenty exhaustion-related genes including ten inhibitory receptors (,*PDCD1, TIGIT, HAVCR2, CD39, CD160, CD244, LAG3, CTLA4, BTLA, C10orf54*) and ten transcriptional

regulators (*TOX, EOMES, GATA3, FOXO1, PRDM1, BATF, IRF4, IRF7, IZKF2, NFATC2*) in our data set and in publicly available data sets for $CD8^+$ T cell exhaustion during LCMV infection (Doering et al., 2012), HIV infection (Quigley et al., 2010) and metastatic melanoma (Baitsch et al., 2011); and separately using KLF2-regulated gene sets defined by a prior report in $CD8^+$ T cells (Preston et al., 2013). T cell receptor beta (*TRB*) complementarity determining region 3 (CDR3) sequences were aligned using MiXCR (Bolotin et al., 2015) and filtered to exclude sequences containing stop codons or alignment gaps. Longitudinal changes in TCR clonotypic composition were calculated as Morisita-Horn dissimilarity ($1 - C_H$) between T3 and T1 samples preceding AC or DC.

Lymphoid tissue microscopy—Formalin-fixed, paraffin-embedded inguinal lymph node tissue sections were stained with polyclonal goat anti-human IgD (Southern Biotech) and polyclonal rabbit anti-human CD8 (Abcam) primary antibodies followed by AlexaFluor 488-conjugated anti-goat IgG and AlexaFluor 750-conjugated anti-rabbit IgG secondary antibodies (R&D Systems). HIV RNA was detected using RNAScope Multiplex Fluorescent Reagent Kit v2 using a Cy5-conjugated HIV *gagpol* probe (Advanced Cell Diagnostics) as per manufacturer's protocol. Fluorescence specificity and background staining were established using manufacturer's negative and positive control staining probes (Advanced Cell Diagnostics) and by staining of an HIV-uninfected lymph node. Stained sections were mounted on coverslips and imaged using a Zeiss Axio Imager Z2 confocal microscope with a 20X objective and a TissueFAXS automated stage. Images were processed using TissueFAXS Viewer (TissueGnostics).

Statistical analyses

Statistical tests were performed using GraphPad Prism v9.0.2 and R. Parametric tests were used for data with normal distributions and nonparametric tests were used for data with non-normal distributions. For data with seven or more replicates, normality was determined using Shapiro-Wilk tests. For data with fewer than seven replicates, normality was estimated by skewness. Where indicated, p values were false discovery rate adjusted (q) using the Benjamini-Hochberg method, p or q values less than 0.05 were considered statistically significant. Figures were prepared using GraphPad Prism v9.0.2 and Adobe Illustrator CC v22.0.1. Graphical abstract was created with BioRender.com. Tables were prepared using Microsoft Word.

Supplementary Material

Refer to Web version on PubMed Central for supplementary material.

ACKNOWLEDGEMENTS

The authors are grateful to study participants; D. Worrall, A. Reissis, O. Carr, F. Ruzicka, S. Ip, A. Millstrom, N. Jilg, H. Heller, Ragon Institute and UCSF SCOPE clinical coordinators for participant recruitment; E. DeMers, K. Judge and Partners IRB for regulatory compliance; Ragon Institute specimen processing and database teams; M. Carrington for *HLA* genotyping; M. Pack, D. Bean, K. Krupp, J. Hitschfel, T. Aicher and D. Koundakjian for technical assistance; V. Viswanadham and P. Jani for preliminary computational analyses; K. Clayton, N. Singh, N. Kaneko, H. Allard-Chamard, V. Mahajan, R. Park and A.-C. Villani for technical advice; A. Khatri and the MGH peptide core facility for peptide synthesis; A. Piechocka-Trocha, M. Waring, T. Diefenbach and the Ragon Institute flow cytometry and imaging core facility staff for operational support; V. Alba and P. Herrero for plasma multi-omics coordination; A. Stryhn, S. Buus, T. Akahoshi and M. Takiguchi for pHLA monomers;

M. Ghebremichael for statistical advice; R. Rutishauser, E. Rodríguez-Gallego and E. Ruiz Mateos for helpful discussions, and Walker lab members for critical evaluation of the research.

This work was supported by funding from Howard Hughes Medical Institute, Bill and Melinda Gates Foundation, Mark and Lisa Schwartz Foundation, Phillip and Susan Ragon Foundation, and the United States National Institutes of Health (NIH) R01 AI149704 to B.D.W.; NIH Extramural LRP-CR to D.R.C.; Fondo de Investigacion Sanitaria (PI16/00503, PI19/01337 and PI20/00326-ISCIII-FEDER), Recera AGUAR (2017SGR948), Spanish AIDS Research Network (RD16/0025/0006-ISCIII-FEDER) and INT20/00031-ISCIII to F.V.; CP19/00146-ISCIII and GeSIDA to A.R.; the CFAR Network of Integrated Clinical Systems (R24 AI067039), Delaney AIDS Research Enterprise (DARE; AI096109, UM1AI126611), and amfAR Institute for HIV Cure Research (amfAR 109301) to S.G.D.; and by the UCSF/Gladstone Institute of Virology & Immunology Center for AIDS Research (CFAR) and Harvard University CFAR (P30 AI027763 to S.G.D. and P30 AI060354 to B.D.W., respectively), which are supported by the following institutes and centers co-funded by and participating with the NIH: NIAID, NCI, NICHD, NHLBI, NIMH, NIA, FIC and OAR. Funders had no role in study design, data collection and analysis, decision to publish or preparation of the manuscript.

REFERENCES

Ahn E, Araki K, Hashimoto M, Li W, Riley JL, Cheung J, Sharpe AH, Freeman GJ, Irving BA, and Ahmed R (2018). Role of PD-1 during effector CD8 T cell differentiation. Proc Natl Acad Sci U S A 115, 4749–4754. 10.1073/pnas.1718217115. [PubMed: 29654146]

Allen TM, Altfeld M, Geer SC, Kalife ET, Moore C, O'Sullivan K M, Desouza I, Feeney ME, Eldridge RL, Maier EL, et al. (2005). Selective escape from CD8+ T-cell responses represents a major driving force of human immunodeficiency virus type 1 (HIV-1) sequence diversity and reveals constraints on HIV-1 evolution. J Virol 79, 13239–13249. 10.1128/JVI.79.21.13239-13249.2005. [PubMed: 16227247]

Altfeld M, Allen TM, Yu XG, Johnston MN, Agrawal D, Korber BT, Montefiori DC, O'Connor DH, Davis BT, Lee PK, et al. (2002). HIV-1 superinfection despite broad CD8+ T-cell responses containing replication of the primary virus. Nature 420, 434–439. 10.1038/nature01200. [PubMed: 12459786]

Bai A, Hu H, Yeung M, and Chen J (2007). Kruppel-like factor 2 controls T cell trafficking by activating L-selectin (CD62L) and sphingosine-1-phosphate receptor 1 transcription. J Immunol 178, 7632–7639. 10.4049/jimmunol.178.12.7632. [PubMed: 17548599]

Bailey JR, Williams TM, Siliciano RF, and Blankson JN (2006). Maintenance of viral suppression in HIV-1-infected HLA-B*57+ elite suppressors despite CTL escape mutations. J Exp Med 203, 1357–1369. 10.1084/jem.20052319. [PubMed: 16682496]

Baitsch L, Baumgaertner P, Devevre E, Raghav SK, Legat A, Barba L, Wieckowski S, Bouzourene H, Deplancke B, Romero P, et al. (2011). Exhaustion of tumor-specific CD8(+) T cells in metastases from melanoma patients. J Clin Invest 121, 2350–2360. 10.1172/JCI46102. [PubMed: 21555851]

Betts MR, Nason MC, West SM, De Rosa SC, Migueles SA, Abraham J, Lederman MM, Benito JM, Goepfert PA, Connors M, et al. (2006). HIV nonprogressors preferentially maintain highly functional HIV-specific CD8+ T cells. Blood 107, 4781–4789. 10.1182/blood-2005-12-4818. [PubMed: 16467198]

Bolotin DA, Poslavsky S, Mitrophanov I, Shugay M, Mamedov IZ, Putintseva EV, and Chudakov DM (2015). MiXCR: software for comprehensive adaptive immunity profiling. Nat Methods 12, 380–381. 10.1038/nmeth.3364. [PubMed: 25924071]

Boritz EA, Darko S, Swaszek L, Wolf G, Wells D, Wu X, Henry AR, Laboune F, Hu J, Ambrozak D, et al. (2016). Multiple Origins of Virus Persistence during Natural Control of HIV Infection. Cell 166, 1004–1015. 10.1016/j.cell.2016.06.039. [PubMed: 27453467]

Borrell M, Fernandez I, Etcheverrry F, Ugarte A, Plana M, Leal L, and Garcia F (2021). High rates of long-term progression in HIV-1-positive elite controllers. J Int AIDS Soc 24, e25675. 10.1002/jia2.25675. [PubMed: 33619912]

Buckley AF, Kuo CT, and Leiden JM (2001). Transcription factor LKLF is sufficient to program T cell quiescence via a c-Myc-dependent pathway. Nat Immunol 2, 698–704. 10.1038/90633. [PubMed: 11477405]

Buggert M, Nguyen S, Salgado-Montes de Oca G, Bengsch B, Darko S, Ransier A, Roberts ER, Del Alcazar D, Brody IB, Vella LA, et al. (2018). Identification and characterization of HIV-

specific resident memory CD8(+) T cells in human lymphoid tissue. Sci Immunol 3. 10.1126/sciimmunol.aar4526.

Chan HY, Zhang J, Garliss CC, Kwaa AK, Blankson JN, and Smith KN (2020). A T Cell Receptor Sequencing-Based Assay Identifies Cross-Reactive Recall CD8(+) T Cell Clonotypes Against Autologous HIV-1 Epitope Variants. Front Immunol 11, 591. 10.3389/fimmu.2020.00591. [PubMed: 32318072]

Chereau F, Madec Y, Sabin C, Obel N, Ruiz-Mateos E, Chrysos G, Fidler S, Lehmann C, Zangerle R, Wittkop L, et al. (2017). Impact of CD4 and CD8 dynamics and viral rebounds on loss of virological control in HIV controllers. PLoS One 12, e0173893. 10.1371/journal.pone.0173893. [PubMed: 28380038]

Chowdhury A, Hayes TL, Bosinger SE, Lawson BO, Vanderford T, Schmitz JE, Paiardini M, Betts M, Chahroudi A, Estes JD, and Silvestri G (2015). Differential Impact of In Vivo CD8+ T Lymphocyte Depletion in Controller versus Progressor Simian Immunodeficiency Virus-Infected Macaques. J Virol 89, 8677–8686. 10.1128/JVI.00869-15. [PubMed: 26063417]

Clayton KL, Collins DR, Lengieza J, Ghebremichael M, Dotiwala F, Lieberman J, and Walker BD (2018). Resistance of HIV-infected macrophages to CD8(+) T lymphocyte-mediated killing drives activation of the immune system. Nat Immunol 19, 475–486. 10.1038/s41590-018-0085-3. [PubMed: 29670239]

Collins DR, Gaiha GD, and Walker BD (2020). CD8(+) T cells in HIV control, cure and prevention. Nat Rev Immunol 20, 471–482. 10.1038/s41577-020-0274-9. [PubMed: 32051540]

Connick E, Folkvord JM, Lind KT, Rakasz EG, Miles B, Wilson NA, Santiago ML, Schmitt K, Stephens EB, Kim HO, et al. (2014). Compartmentalization of simian immunodeficiency virus replication within secondary lymphoid tissues of rhesus macaques is linked to disease stage and inversely related to localization of virus-specific CTL. J Immunol 193, 5613–5625. 10.4049/jimmunol.1401161. [PubMed: 25362178]

Connick E, Mattila T, Folkvord JM, Schlichtemeier R, Meditz AL, Ray MG, McCarter MD, Mawhinney S, Hage A, White C, and Skinner PJ (2007). CTL fail to accumulate at sites of HIV-1 replication in lymphoid tissue. J Immunol 178, 6975–6983. 10.4049/jimmunol.178.11.6975. [PubMed: 17513747]

Day CL, Kaufmann DE, Kiepiela P, Brown JA, Moodley ES, Reddy S, Mackey EW, Miller JD, Leslie AJ, DePierres C, et al. (2006). PD-1 expression on HIV-specific T cells is associated with T-cell exhaustion and disease progression. Nature 443, 350–354. 10.1038/nature05115. [PubMed: 16921384]

Doering TA, Crawford A, Angelosanto JM, Paley MA, Ziegler CG, and Wherry EJ (2012). Network analysis reveals centrally connected genes and pathways involved in CD8+ T cell exhaustion versus memory. Immunity 37, 1130–1144. 10.1016/j.immuni.2012.08.021. [PubMed: 23159438]

Edgar RC (2004). MUSCLE: multiple sequence alignment with high accuracy and high throughput. Nucleic Acids Res 32, 1792–1797. 10.1093/nar/gkh340. [PubMed: 15034147]

Estes JD, Kityo C, Ssali F, Swainson L, Makamdop KN, Del Prete GQ, Deeks SG, Luciw PA, Chipman JG, Beilman GJ, et al. (2017). Defining total-body AIDS-virus burden with implications for curative strategies. Nat Med 23, 1271–1276. 10.1038/nm.4411. [PubMed: 28967921]

Fenwick C, Joo V, Jacquier P, Noto A, Banga R, Perreau M, and Pantaleo G (2019). T-cell exhaustion in HIV infection. Immunol Rev 292, 149–163. 10.1111/imr.12823. [PubMed: 31883174]

Friedrich TC, Valentine LE, Yant LJ, Rakasz EG, Piaskowski SM, Furlott JR, Weisgrau KL, Burwitz B, May GE, Leon EJ, et al. (2007). Subdominant CD8+ T-cell responses are involved in durable control of AIDS virus replication. J Virol 81, 3465–3476. 10.1128/JVI.02392-06. [PubMed: 17251286]

Fukazawa Y, Lum R, Okoye AA, Park H, Matsuda K, Bae JY, Hagen SI, Shoemaker R, Deleage C, Lucero C, et al. (2015). B cell follicle sanctuary permits persistent productive simian immunodeficiency virus infection in elite controllers. Nat Med 21, 132–139. 10.1038/nm.3781. [PubMed: 25599132]

Gaiha GD, McKim KJ, Woods M, Pertel T, Rohrbach J, Barteneva N, Chin CR, Liu D, Soghoian DZ, Cesa K, et al. (2014). Dysfunctional HIV-specific CD8+ T cell proliferation is associated with increased caspase-8 activity and mediated by necroptosis. Immunity 41, 1001–1012. 10.1016/j.immuni.2014.12.011. [PubMed: 25526311]

Gaiha GD, Rossin EJ, Urbach J, Landeros C, Collins DR, Nwonu C, Muzhingi I, Anahtar MN, Waring OM, Piechocka-Trocha A, et al. (2019). Structural topology defines protective CD8(+) T cell epitopes in the HIV proteome. Science 364, 480–484. 10.1126/science.aav5095. [PubMed: 31048489]

Goulder PJ, Phillips RE, Colbert RA, McAdam S, Ogg G, Nowak MA, Giangrande P, Luzzi G, Morgan B, Edwards A, et al. (1997). Late escape from an immunodominant cytotoxic T-lymphocyte response associated with progression to AIDS. Nat Med 3, 212–217. 10.1038/nm0297-212. [PubMed: 9018241]

Gouy M, Guindon S, and Gascuel O (2010). SeaView version 4: A multiplatform graphical user interface for sequence alignment and phylogenetic tree building. Mol Biol Evol 27, 221–224. 10.1093/molbev/msp259. [PubMed: 19854763]

Grabar S, Selinger-Leneman H, Abgrall S, Pialoux G, Weiss L, and Costagliola D (2017). Loss of long-term non-progressor and HIV controller status over time in the French Hospital Database on HIV - ANRS CO4. PLoS One 12, e0184441. 10.1371/journal.pone.0184441. [PubMed: 28968404]

Guindon S, Dufayard JF, Lefort V, Anisimova M, Hordijk W, and Gascuel O (2010). New algorithms and methods to estimate maximum-likelihood phylogenies: assessing the performance of PhyML 3.0. Syst Biol 59, 307–321. 10.1093/sysbio/syq010. [PubMed: 20525638]

Hanzelmann S, Castelo R, and Guinney J (2013). GSVA: gene set variation analysis for microarray and RNA-seq data. BMC Bioinformatics 14, 7. 10.1186/1471-2105-14-7. [PubMed: 23323831]

He R, Hou S, Liu C, Zhang A, Bai Q, Han M, Yang Y, Wei G, Shen T, Yang X, et al. (2016). Follicular CXCR5- expressing CD8(+) T cells curtail chronic viral infection. Nature 537, 412–428. 10.1038/nature19317. [PubMed: 27501245]

Henn MR, Boutwell CL, Charlebois P, Lennon NJ, Power KA, Macalalad AR, Berlin AM, Malboeuf CM, Ryan EM, Gnerre S, et al. (2012). Whole genome deep sequencing of HIV-1 reveals the impact of early minor variants upon immune recognition during acute infection. PLoS Pathog 8, e1002529. 10.1371/journal.ppat.1002529. [PubMed: 22412369]

Hersperger AR, Pereyra F, Nason M, Demers K, Sheth P, Shin LY, Kovacs CM, Rodriguez B, Sieg SF, Teixeira-Johnson L, et al. (2010). Perforin expression directly ex vivo by HIV-specific CD8 T-cells is a correlate of HIV elite control. PLoS Pathog 6, e1000917. 10.1371/journal.ppat.1000917. [PubMed: 20523897]

Jiang C, Lian X, Gao C, Sun X, Einkauf KB, Chevalier JM, Chen SMY, Hua S, Rhee B, Chang K, et al. (2020). Distinct viral reservoirs in individuals with spontaneous control of HIV-1. Nature 585, 261–267. 10.1038/s41586-020-2651-8. [PubMed: 32848246]

Kall L, Canterbury JD, Weston J, Noble WS, and MacCoss MJ (2007). Semi-supervised learning for peptide identification from shotgun proteomics datasets. Nat Methods 4, 923–925. 10.1038/nmeth1113. [PubMed: 17952086]

Koofhethile CK, Ndhlovu ZM, Thobakgale-Tshabalala C, Prado JG, Ismail N, Mncube Z, Mkhize L, van der Stok M, Yende N, Walker BD, et al. (2016). CD8+ T Cell Breadth and Ex Vivo Virus Inhibition Capacity Distinguish between Viremic Controllers with and without Protective HLA Class I Alleles. J Virol 90, 6818–6831. 10.1128/JVI.00276-16. [PubMed: 27194762]

Kuo CT, Veselits ML, and Leiden JM (1997). LKLF: A transcriptional regulator of single-positive T cell quiescence and survival. Science 277, 1986–1990. 10.1126/science.277.5334.1986. [PubMed: 9302292]

Lee GQ, Orlova-Fink N, Einkauf K, Chowdhury FZ, Sun X, Harrington S, Kuo HH, Hua S, Chen HR, Ouyang Z, et al. (2017). Clonal expansion of genome-intact HIV-1 in functionally polarized Th1 CD4+ T cells. J Clin Invest 127, 2689–2696. 10.1172/JCI93289. [PubMed: 28628034]

Lee JY, Skon CN, Lee YJ, Oh S, Taylor JJ, Malhotra D, Jenkins MK, Rosenfeld MG, Hogquist KA, and Jameson SC (2015). The transcription factor KLF2 restrains CD4(+) T follicular helper cell differentiation. Immunity 42, 252–264. 10.1016/j.immuni.2015.01.013. [PubMed: 25692701]

Lee WP, Stromberg MP, Ward A, Stewart C, Garrison EP, and Marth GT (2014). MOSAIK: a hash-based algorithm for accurate next-generation sequencing short-read mapping. PLoS One 9, e90581. 10.1371/journal.pone.0090581. [PubMed: 24599324]

Leon A, Perez I, Ruiz-Mateos E, Benito JM, Leal M, Lopez-Galindez C, Rallon N, Alcami J, Lopez-Aldeguer J, Viciana P, et al. (2016). Rate and predictors of progression in elite and viremic HIV-1 controllers. AIDS 30, 1209–1220. 10.1097/QAD.0000000000001050. [PubMed: 26854807]

Leong YA, Chen Y, Ong HS, Wu D, Man K, Deleage C, Minnich M, Meckiff BJ, Wei Y, Hou Z, et al. (2016). CXCR5(+) follicular cytotoxic T cells control viral infection in B cell follicles. Nat Immunol 17, 1187–1196. 10.1038/ni.3543. [PubMed: 27487330]

Li B, and Dewey CN (2011). RSEM: accurate transcript quantification from RNA-Seq data with or without a reference genome. BMC Bioinformatics 12, 323. 10.1186/1471-2105-12-323. [PubMed: 21816040]

Liberzon A, Subramanian A, Pinchback R, Thorvaldsdottir H, Tamayo P, and Mesirov JP (2011). Molecular signatures database (MSigDB) 3.0. Bioinformatics 27, 1739–1740. 10.1093/bioinformatics/btr260. [PubMed: 21546393]

Llano A, Cedeño S, Arrieta SS, and Brander C (2019). The 2019 Optimal HIV CTL epitopes update : Growing diversity in epitope length and HLA restriction. HIV Molecular Immunology. Los Alamos National Laboratory.

Love MI, Huber W, and Anders S (2014). Moderated estimation of fold change and dispersion for RNA-seq data with DESeq2. Genome Biol 15, 550. 10.1186/s13059-014-0550-8. [PubMed: 25516281]

Madec Y, Boufassa F, Porter K, Prins M, Sabin C, d'Arminio Monforte A, Amornkul P, Bartmeyer B, Sannes M, Venet A, et al. (2013). Natural history of HIV-control since seroconversion. AIDS 27, 2451–2460. 10.1097/01.aids.0000431945.72365.01. [PubMed: 23912979]

McLane LM, Abdel-Hakeem MS, and Wherry EJ (2019). CD8 T Cell Exhaustion During Chronic Viral Infection and Cancer. Annu Rev Immunol 37, 457–495. 10.1146/annurev-immunol-041015-055318. [PubMed: 30676822]

Migueles SA, and Connors M (2015). Success and failure of the cellular immune response against HIV-1. Nat Immunol 16, 563–570. 10.1038/ni.3161. [PubMed: 25988888]

Migueles SA, Laborico AC, Shupert WL, Sabbaghian MS, Rabin R, Hallahan CW, Van Baarle D, Kostense S, Miedema F, McLaughlin M, et al. (2002). HIV-specific CD8+ T cell proliferation is coupled to perforin expression and is maintained in nonprogressors. Nat Immunol 3, 1061–1068. 10.1038/ni845. [PubMed: 12368910]

Migueles SA, Osborne CM, Royce C, Compton AA, Joshi RP, Weeks KA, Rood JE, Berkley AM, Sacha JB, Cogliano-Shutta NA, et al. (2008). Lytic granule loading of CD8+ T cells is required for HIV-infected cell elimination associated with immune control. Immunity 29, 1009–1021. 10.1016/j.immuni.2008.10.010. [PubMed: 19062316]

Migueles SA, Rogan DC, Gavil NV, Kelly EP, Toulmin SA, Wang LT, Lack J, Ward AJ, Pryal PF, Ludwig AK, et al. (2020). Antigenic Restimulation of Virus-Specific Memory CD8(+) T Cells Requires Days of Lytic Protein Accumulation for Maximal Cytotoxic Capacity. J Virol 94. 10.1128/JVI.01595-20.

Migueles SA, Weeks KA, Nou E, Berkley AM, Rood JE, Osborne CM, Hallahan CW, Cogliano-Shutta NA, Metcalf JA, McLaughlin M, et al. (2009). Defective human immunodeficiency virus-specific CD8+ T-cell polyfunctionality, proliferation, and cytotoxicity are not restored by antiretroviral therapy. J Virol 83, 11876–11889. 10.1128/JVI.01153-09. [PubMed: 19726501]

Miura T, Brumme CJ, Brockman MA, Brumme ZL, Pereyra F, Block BL, Trocha A, John M, Mallal S, Harrigan PR, and Walker BD (2009). HLA-associated viral mutations are common in human immunodeficiency virus type 1 elite controllers. J Virol 83, 3407–3412. 10.1128/JVI.02459-08. [PubMed: 19153230]

Ndhlovu ZM, Chibnik LB, Proudfoot J, Vine S, McMullen A, Cesa K, Porichis F, Jones RB, Alvino DM, Hart MG, et al. (2013). High-dimensional immunomonitoring models of HIV-1-specific CD8 T-cell responses accurately identify subjects achieving spontaneous viral control. Blood 121, 801–811. 10.1182/blood-2012-06-436295. [PubMed: 23233659]

Nguyen S, Deleage C, Darko S, Ransier A, Truong DP, Agarwal D, Japp AS, Wu VH, Kuri-Cervantes L, Abdel-Mohsen M, et al. (2019). Elite control of HIV is associated with distinct functional and transcriptional signatures in lymphoid tissue CD8(+) T cells. Sci Transl Med 11. 10.1126/scitranslmed.aax4077.

Noel N, Lerolle N, Lecuroux C, Goujard C, Venet A, Saez-Cirion A, Avettand-Fenoel V, Meyer L, Boufassa F, Lambotte O, and Group, A.C.C.S. (2015). Immunologic and Virologic Progression in HIV Controllers: The Role of Viral ″Blips″ and Immune Activation in the ANRS CO21 CODEX Study. PLoS One 10, e0131922. 10.1371/journal.pone.0131922. [PubMed: 26146823]

Papagno L, Spina CA, Marchant A, Salio M, Rufer N, Little S, Dong T, Chesney G, Waters A, Easterbrook P, et al. (2004). Immune activation and CD8+ T-cell differentiation towards senescence in HIV-1 infection. PLoS Biol 2, E20. 10.1371/journal.pbio.0020020. [PubMed: 14966528]

Pereyra F, Jia X, McLaren PJ, Telenti A, de Bakker PI, Walker BD, Ripke S, Brumme CJ, Pulit SL, Carrington M, et al. (2010). The major genetic determinants of HIV-1 control affect HLA class I peptide presentation. Science 330, 1551–1557. 10.1126/science.1195271. [PubMed: 21051598]

Pernas M, Tarancon-Diez L, Rodriguez-Gallego E, Gomez J, Prado JG, Casado C, Dominguez-Molina B, Olivares I, Coiras M, Leon A, et al. (2018). Factors Leading to the Loss of Natural Elite Control of HIV-1 Infection. J Virol 92. 10.1128/JVI.01805-17.

Perreau M, Savoye AL, De Crignis E, Corpataux JM, Cubas R, Haddad EK, De Leval L, Graziosi C, and Pantaleo G (2013). Follicular helper T cells serve as the major CD4 T cell compartment for HIV-1 infection, replication, and production. J Exp Med 210, 143–156. 10.1084/jem.20121932. [PubMed: 23254284]

Petrovas C, Casazza JP, Brenchley JM, Price DA, Gostick E, Adams WC, Precopio ML, Schacker T, Roederer M, Douek DC, and Koup RA (2006). PD-1 is a regulator of virus-specific CD8+ T cell survival in HIV infection. J Exp Med 203, 2281–2292. 10.1084/jem.20061496. [PubMed: 16954372]

Pohlmeyer CW, Buckheit RW 3rd, Siliciano RF, and Blankson JN (2013). CD8+ T cells from HLA-B*57 elite suppressors effectively suppress replication of HIV-1 escape mutants. Retrovirology 10, 152. 10.1186/1742-4690-10-152. [PubMed: 24330837]

Preston GC, Feijoo-Carnero C, Schurch N, Cowling VH, and Cantrell DA (2013). The impact of KLF2 modulation on the transcriptional program and function of CD8 T cells. PLoS One 8, e77537. 10.1371/journal.pone.0077537. [PubMed: 24155966]

Quigley M, Pereyra F, Nilsson B, Porichis F, Fonseca C, Eichbaum Q, Julg B, Jesneck JL, Brosnahan K, Imam S, et al. (2010). Transcriptional analysis of HIV-specific CD8+ T cells shows that PD-1 inhibits T cell function by upregulating BATF. Nat Med 16, 1147–1151. 10.1038/nm.2232. [PubMed: 20890291]

Reuter MA, Del Rio Estrada PM, Buggert M, Petrovas C, Ferrando-Martinez S, Nguyen S, Sada Japp A, Ablanedo-Terrazas Y, Rivero-Arrieta A, Kuri-Cervantes L, et al. (2017). HIV-Specific CD8(+) T Cells Exhibit Reduced and Differentially Regulated Cytolytic Activity in Lymphoid Tissue. Cell Rep 21, 3458–3470. 10.1016/j.celrep.2017.11.075. [PubMed: 29262326]

Ritchie ME, Phipson B, Wu D, Hu Y, Law CW, Shi W, and Smyth GK (2015). limma powers differential expression analyses for RNA-sequencing and microarray studies. Nucleic Acids Res 43, e47. 10.1093/nar/gkv007. [PubMed: 25605792]

Rodriguez-Gallego E, Tarancon-Diez L, Garcia F, Del Romero J, Benito JM, Alba V, Herrero P, Rull A, Dominguez-Molina B, Martinez-Madrid O, et al. (2019). Proteomic Profile Associated With Loss of Spontaneous Human Immunodeficiency Virus Type 1 Elite Control. J Infect Dis 219, 867–876. 10.1093/infdis/jiy599. [PubMed: 30312441]

Rogan DC, and Connors M (2021). Immunologic Control of HIV-1: What Have We Learned and Can We Induce It? Curr HIV/AIDS Rep. 10.1007/s11904-021-00545-2.

Rosas-Umbert M, Llano A, Bellido R, Olvera A, Ruiz-Riol M, Rocafort M, Fernandez MA, Cobarsi P, Crespo M, Dorrell L, et al. (2019). Mechanisms of Abrupt Loss of Virus Control in a Cohort of Previous HIV Controllers. J Virol 93. 10.1128/JVI.01436-18.

Rossjohn J, Gras S, Miles JJ, Turner SJ, Godfrey DI, and McCluskey J (2015). T cell antigen receptor recognition of antigen-presenting molecules. Annu Rev Immunol 33, 169–200. 10.1146/annurev-immunol-032414-112334. [PubMed: 25493333]

Rutishauser RL, Deguit CDT, Hiatt J, Blaeschke F, Roth TL, Wang L, Raymond KA, Starke CE, Mudd JC, Chen W, et al. (2021). TCF-1 regulates HIV-specific CD8+ T cell expansion capacity. JCI Insight 6. 10.1172/jci.insight.136648.

Saez-Cirion A, Lacabaratz C, Lambotte O, Versmisse P, Urrutia A, Boufassa F, Barre-Sinoussi F, Delfraissy JF, Sinet M, Pancino G, et al. (2007). HIV controllers exhibit potent CD8 T cell capacity to suppress HIV infection ex vivo and peculiar cytotoxic T lymphocyte activation phenotype. Proc Natl Acad Sci U S A 104, 6776–6781. 10.1073/pnas.0611244104. [PubMed: 17428922]

Schober SL, Kuo CT, Schluns KS, Lefrancois L, Leiden JM, and Jameson SC (1999). Expression of the transcription factor lung Kruppel-like factor is regulated by cytokines and correlates with survival of memory T cells in vitro and in vivo. J Immunol 163, 3662–3667. [PubMed: 10490960]

Sekine T, Perez-Potti A, Nguyen S, Gorin JB, Wu VH, Gostick E, Llewellyn-Lacey S, Hammer Q, Falck-Jones S, Vangeti S, et al. (2020). TOX is expressed by exhausted and polyfunctional human effector memory CD8(+) T cells. Sci Immunol 5. 10.1126/sciimmunol.aba7918.

Tarancon-Diez L, Rodriguez-Gallego E, Rull A, Peraire J, Vilades C, Portilla I, Jimenez-Leon MR, Alba V, Herrero P, Leal M, et al. (2019). Immunometabolism is a key factor for the persistent spontaneous elite control of HIV-1 infection. EBioMedicine 42, 86–96. 10.1016/j.ebiom.2019.03.004. [PubMed: 30879922]

Trautmann L, Janbazian L, Chomont N, Said EA, Gimmig S, Bessette B, Boulassel MR, Delwart E, Sepulveda H, Balderas RS, et al. (2006). Upregulation of PD-1 expression on HIV-specific CD8+ T cells leads to reversible immune dysfunction. Nat Med 12, 1198–1202. 10.1038/nm1482. [PubMed: 16917489]

Tully DC, Ogilvie CB, Batorsky RE, Bean DJ, Power KA, Ghebremichael M, Bedard HE, Gladden AD, Seese AM, Amero MA, et al. (2016). Differences in the Selection Bottleneck between Modes of Sexual Transmission Influence the Genetic Composition of the HIV-1 Founder Virus. PLoS Pathog 12, e1005619. 10.1371/journal.ppat.1005619. [PubMed: 27163788]

Villani AC, and Shekhar K (2017). Single-Cell RNA Sequencing of Human T Cells. Methods Mol Biol 1514, 203–239. 10.1007/978-1-4939-6548-9_16. [PubMed: 27787803]

Wang K, and Fingert JH (2012). Statistical tests for detecting rare variants using variance-stabilising transformations. Ann Hum Genet 76, 402–409. 10.1111/j.1469-1809.2012.00718.x. [PubMed: 22724536]

Weber JP, Fuhrmann F, Feist RK, Lahmann A, Al Baz MS, Gentz LJ, Vu Van D, Mages HW, Haftmann C, Riedel R, et al. (2015). ICOS maintains the T follicular helper cell phenotype by down-regulating Kruppel-like factor 2. J Exp Med 212, 217–233. 10.1084/jem.20141432. [PubMed: 25646266]

Yang OO, Cumberland WG, Escobar R, Liao D, and Chew KW (2017). Demographics and natural history of HIV-1-infected spontaneous controllers of viremia. AIDS 31, 1091–1098. 10.1097/QAD.0000000000001443. [PubMed: 28301422]

Yang X, Charlebois P, Gnerre S, Coole MG, Lennon NJ, Levin JZ, Qu J, Ryan EM, Zody MC, and Henn MR (2012). De novo assembly of highly diverse viral populations. BMC Genomics 13, 475. 10.1186/1471-2164-13-475. [PubMed: 22974120]

Yang X, Charlebois P, Macalalad A, Henn MR, and Zody MC (2013). V-Phaser 2: variant inference for viral populations. BMC Genomics 14, 674. 10.1186/1471-2164-14-674. [PubMed: 24088188]

Zyla J, Marczyk M, Domaszewska T, Kaufmann SHE, Polanska J, and Weiner J (2019). Gene set enrichment for reproducible science: comparison of CERNO and eight other algorithms. Bioinformatics 35, 5146–5154. 10.1093/bioinformatics/btz447. [PubMed: 31165139]

HIGHLIGHTS

- Longitudinal evaluation of 34 subjects with durable or aborted spontaneous HIV control
- Recognition of autologous HIV by T cell receptors is maintained during aborted control
- HIV-specific $CD8^+$ T cell proliferation and cytotoxicity wane prior to aborted control
- Elevated *KLF2* without hallmarks of exhaustion observed in functionally impaired T cells

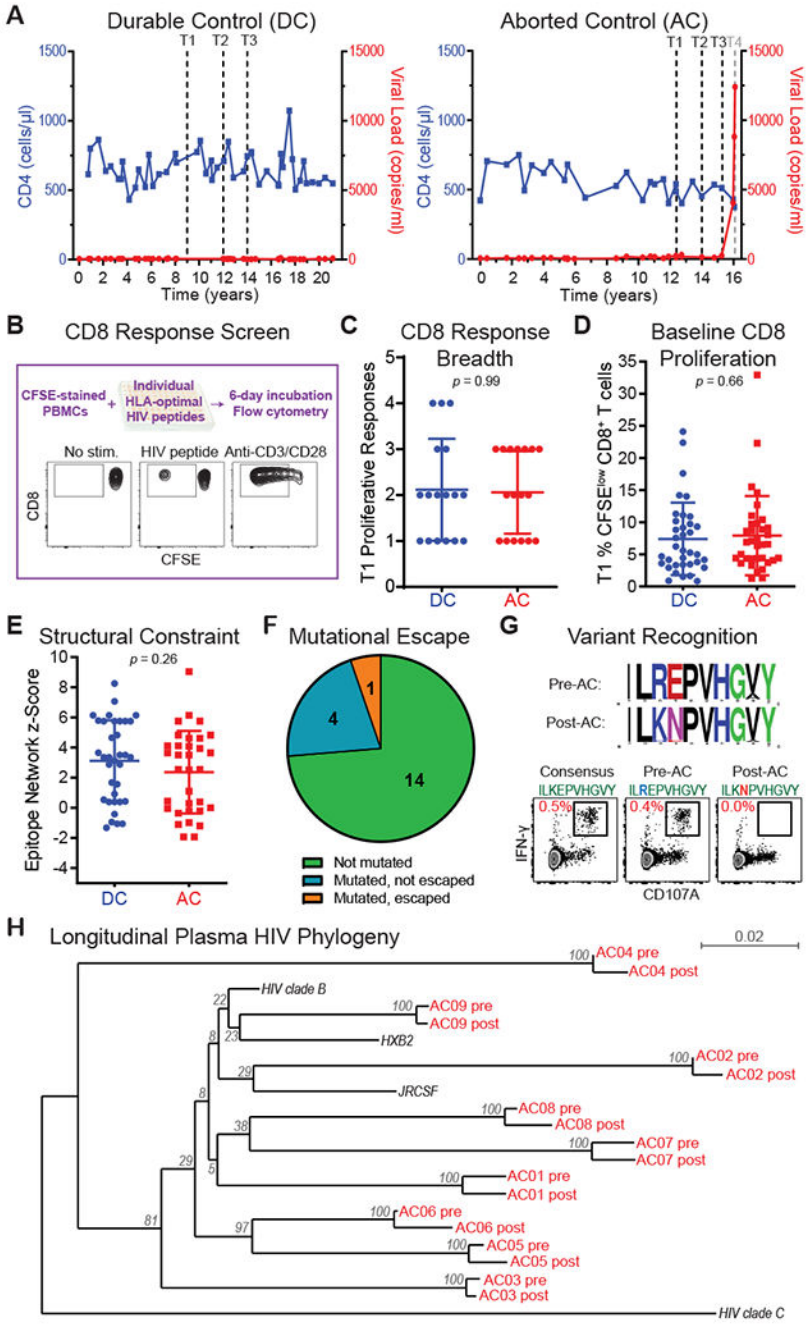

Figure 1: HIV-specific CD8$^+$ T cells maintain recognition of autologous HIV during aborted viral control.

(A) Viral loads (right axes) and CD4 counts (left axes) for representative subjects with durable control (DC) or aborted control (AC) of HIV viremia. Longitudinal samples T1-T3 (dashed lines) precede loss or maintenance of viral control. **(B)** Schematic of and representative results from proliferation screen for HIV epitope-specific CD8$^+$ T cell responses comparing carboxyfluorescein succinimidyl ester (CFSE) dilution in response to unstimulated negative control, individual HLA-optimal HIV peptide stimulated, and

anti-CD3/CD28 stimulated positive control. **(C)** Number (breadth) of HIV peptide-specific proliferative $CD8^+$ T cell responses detected above background at baseline (T1) in subjects with AC or DC (n = 17 each; Mann-Whitney U-test). **(D)** Frequency of CFSE-low $CD8^+$ T cells after stimulation with individual HLA-optimal HIV peptides at baseline (T1) in subjects with AC or DC (n = 36 and 35 responses, respectively, among 17 subjects each; unpaired t test). **(E)** HIV epitope network z-scores, where available, for proliferative HIV-specific responses detected in subjects with DC or AC (n = 35 and 33 responses, respectively, among 17 subjects each; unpaired t test). **(F)** Summary of mutations and escape from $CD8^+$ T cell recognition in 19 responses from 10 subjects with AC. **(G)** Weblogos depicting longitudinal variation observed in a $CD8^+$ T cell epitope sequence targeted by subject AC07 before and after aborted control of viremia (top). Recognition of clade B consensus, pre-AC and post-AC sequence variant peptides after 4-hour stimulation of PBMCs collected prior to AC, as measured by flow cytometry of surface CD107A and intracellular IFN-γ (bottom). **(H)** Maximum likelihood phylogenetic tree showing genetic distances between plasma HIV sequences from the indicated subjects before (pre) and after (post) AC, and reference HIV sequences. Values in gray represent percentage of 1000 bootstraps for each branch. See also Figures S1-S2 and Tables S1-S3.

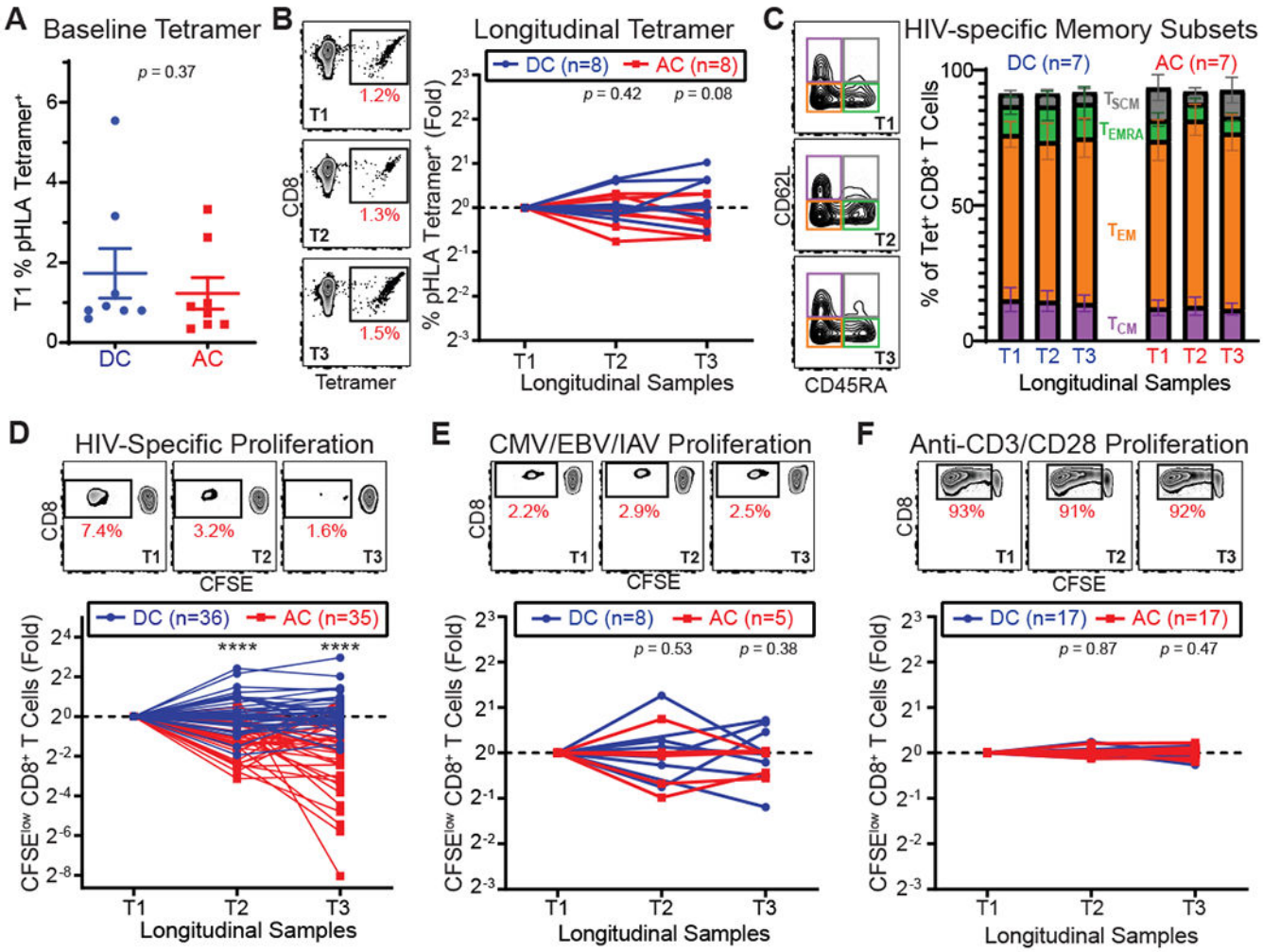

Figure 2: HIV-specific CD8$^+$ T cell proliferation is progressively and selectively impaired preceding aborted viral control.

(A) Summary of peptide-HLA (pHLA) tetramer staining frequencies at baseline (T1) in DC ($n = 8$) and AC ($n = 8$) measured by flow cytometry; Mann-Whitney U-test. **(B)** Representative longitudinal HIV-specific pH LA tetramer staining preceding AC (left). Summary of longitudinal changes in HIV-specific CD8$^+$ T cell frequencies preceding AC or DC (right); unpaired t tests. **(C)** Representative longitudinal bulk CD8$^+$ T cell memory subset composition measured by flow cytometric evaluation of CD45RA and CD62L surface expression (left). Summary of longitudinal bulk CD8$^+$ T cell memory subset frequencies (right), represented as mean +/− SEM. T_{CM} = central memory, T_{EM} = effector memory, T_{EMRA} = effector memory CD45RA$^+$, T_{SCM} = stem cell-like memory. **(D)** Representative CD8$^+$ T cell proliferation assay results preceding AC following 6-day stimulation with HLA-optimal HIV peptide (above). Summary of longitudinal changes in HIV antigen-specific proliferation in response to stimulation with individual HLA-optimal HIV peptides preceding AC or DC for the indicated number of responses in 17 subjects from each group (below). **** $p < 0.0001$, Mann-Whitney U-tests. **(E)** Representative CD8$^+$ T cell proliferation assay results (above) and summary of longitudinal changes in

proliferation (below) following stimulation with pooled CMV, EBV and IAV peptides at longitudinal time points preceding AC or DC; unpaired t tests. **(F)** Representative $CD8^+$ T cell proliferation assay results (above) and summary of longitudinal changes in proliferation (below) following stimulation with anti-CD3 and anti-CD28 antibodies at longitudinal time points preceding AC or DC; unpaired t tests. Values shown as fold over baseline (T1) where indicated to highlight longitudinal changes. See also Figures S3-S4.

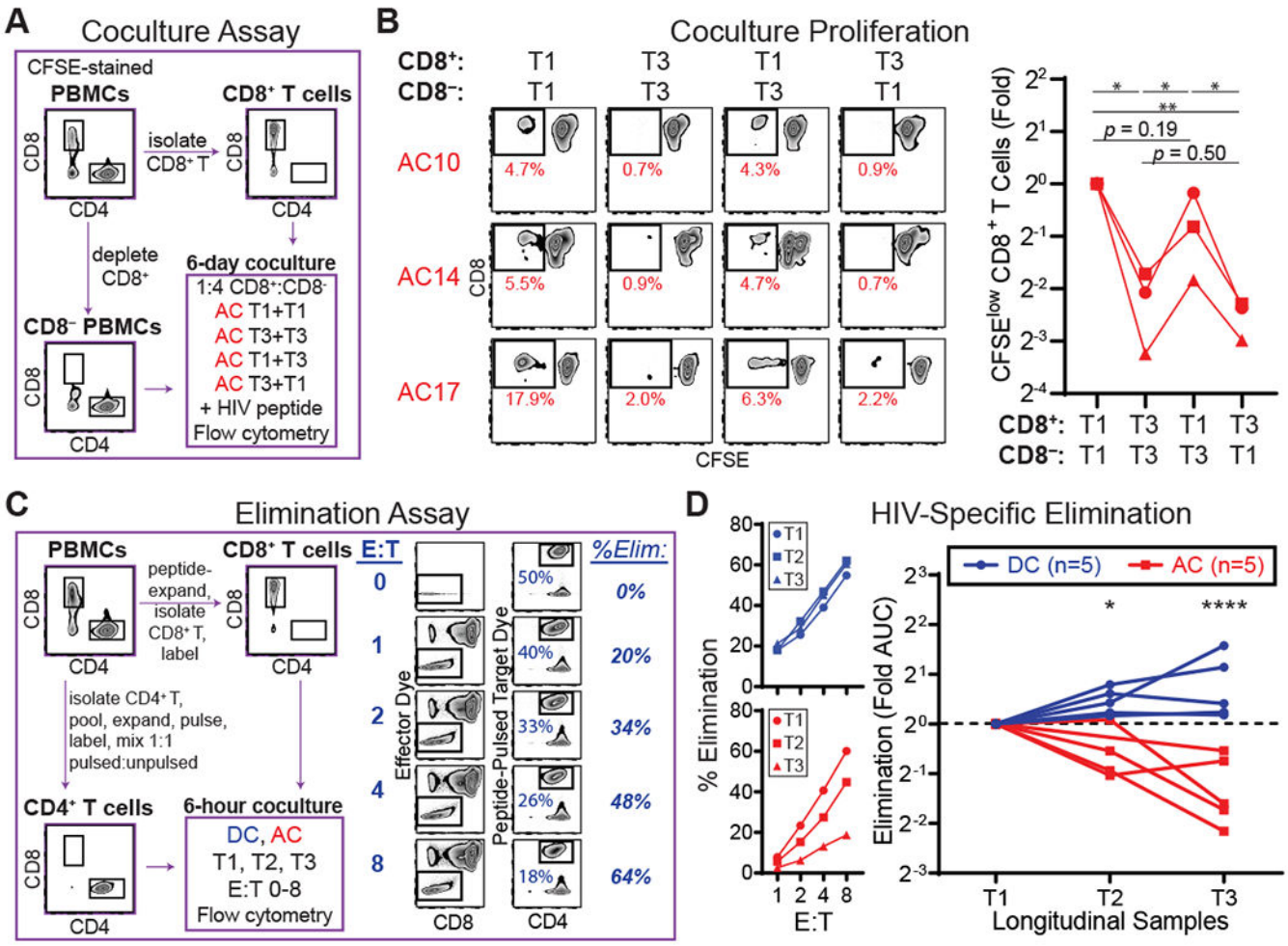

Figure 3: Proliferative and cytolytic defects preceding aborted HIV control are CD8$^+$ T cell intrinsic.

(A) Schematic of coculture proliferation assay in which HIV peptide-expanded CD8$^+$ T cells from time points T1 or T3 preceding AC were cocultured with CD8-depleted PBMCs from time points T1 or T3 and stimulated with HIV peptide for 6 days. **(B)** Flow cytometry results (left) and baseline-normalized summary (right) of HIV-specific proliferation following cocultures from 3 subjects preceding AC. * $p < 0.05$, ** $p < 0.01$, ratio-paired t tests. **(C)** Schematic (left) of elimination assay in which CD8$^+$ T cells from time points T1-T3 were individually cocultured with 50% HIV peptide-pulsed autologous CD4$^+$ T cells for 6 hours at effector:target (E:T) ratios of 0, 1, 2, 4 and 8. Cells were gated as shown (right) to calculate percent of residual peptide-pulsed and percent elimination (relative to E:T 0). **(D)** Representative killing curves measuring elimination of autologous HIV peptide-pulsed CD4$^+$ T cells by HIV peptide-expanded CD8$^+$ T cells from longitudinal time points preceding AC or DC at E:T 1-8 (left). Summary of longitudinal changes in HIV-specific elimination, measured as area under killing curve (AUC) and normalized for baseline (T1) preceding AC or DC (right). * $p < 0.05$, **** $p < 0.0001$, unpaired t tests.

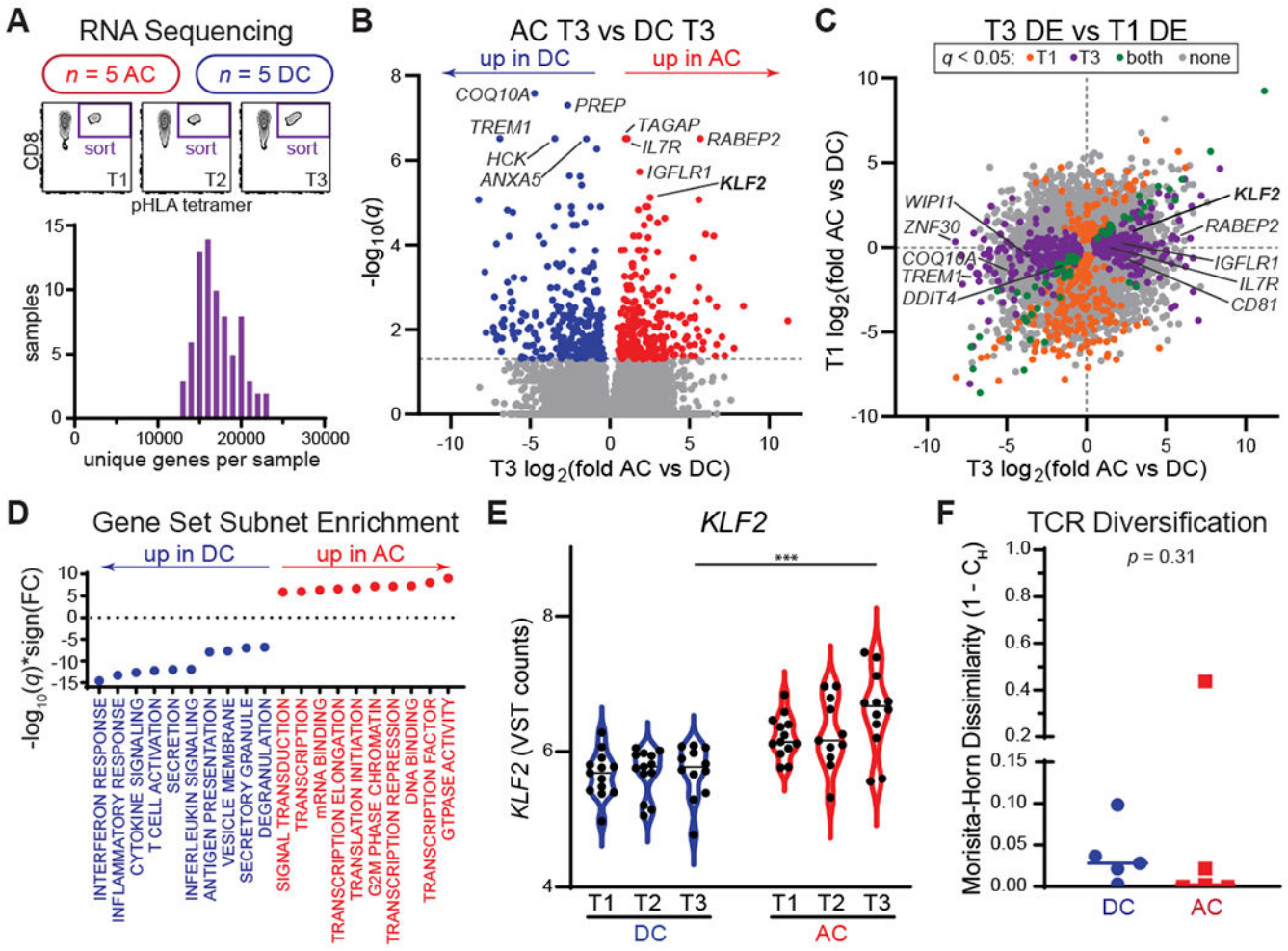

Figure 4: Transcriptional profiles of HIV-specific CD8$^+$ T cells are altered preceding aborted viral control.

(A) Schematic overview of RNA-seq from longitudinal HIV-specific CD8$^+$ T cells preceding AC (n = 5) or DC (n = 5) isolated by FACS (top). Histogram showing number of unique genes detected per sample (bottom). **(B)** Volcano plot summarizing differential gene expression at time point T3 preceding AC (n = 5) versus DC (n = 5). The top five most significant up- and down-regulated genes are labeled. **(C)** Plot comparing differential expression at baseline (T1, y-axis) and time point T3 (x-axis) preceding AC (n = 5) versus DC (n = 5). Genes are colored by significance (q < 0.05) for each comparison. The top five most significant up- and down-regulated genes unique to T3 are labeled. **(D)** Summary of gene set subnet enrichment analyses of differentially expressed genes from B ranked by FDR-adjusted q, signed by direction of fold change in AC vs DC (top 10 shown for each direction). **(E)** Violin plot summarizing longitudinal *KLF2* mRNA expression as normalized, variance stabilizing transformed (VST) counts preceding AC (n = 5) or DC (n = 5). *** p < 0.001, unpaired t test. **(F)** Summary of longitudinal TCR clonotypic diversification as Morisita-Horn dissimilarity between T3 and T1 preceding AC (n = 5) or DC (n = 5); unpaired t test. See also Figures S5-S6 and Tables S4-S5.

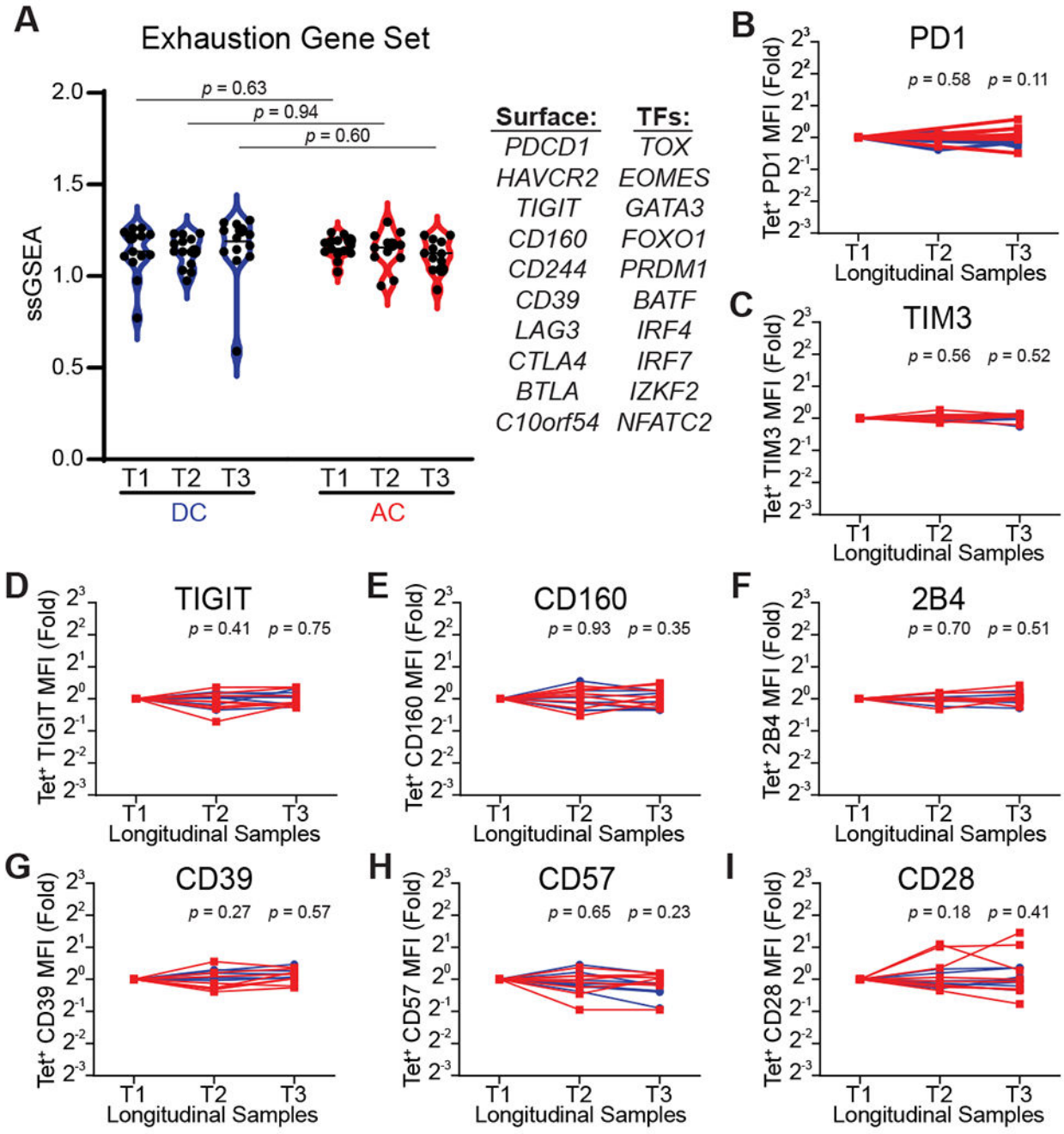

Figure 5: Functional impairment preceding aborted HIV control is distinct from T cell exhaustion and senescence.

(A) Violin plot summarizing longitudinal single-sample gene set enrichment analyses (ssGSEA) for the listed set of exhaustion-associated genes preceding AC ($n = 5$) or DC ($n = 5$); unpaired t tests. **(B-I)** Summary of longitudinal changes in surface flow cytometric median fluorescence intensities (MFI) on HIV-specific $CD8^+$ T cells normalized for baseline (T1) preceding AC ($n = 8$) or DC ($n = 7$) for PD1 (B), TIM3 (C), TIGIT (D), CD160 (E), 2B4 (F), CD39 (G), CD57 (H) and CD28 (I); unpaired t tests. See also Figure S7.

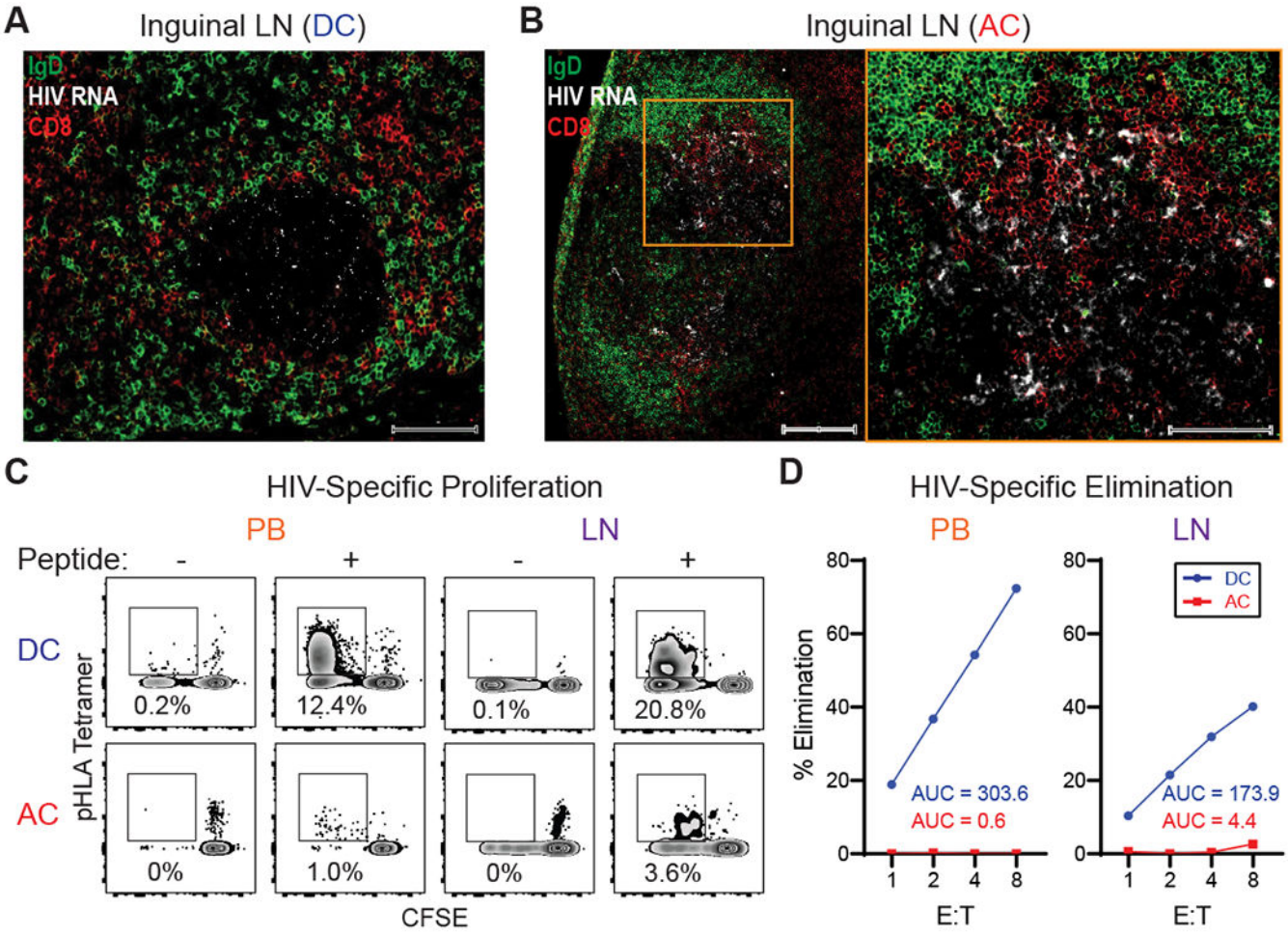

Figure 6: Lymphoid HIV-specific CD8$^+$ T cells are functionally impaired during aborted viral control.

(A-B) Composite immunofluorescence micrographs depicting inguinal lymph node follicular margins (IgD, green), CD8$^+$ cells (red) and HIV RNA via fluorescent probes (white) in sections from specimens obtained from one subject each during DC (A) or AC (B) for qualitative comparison. Orange box represents inset, scale bars represent 100 μm. (C) CD8$^+$ T cell proliferation without (−) and with (+) 6-day HIV peptide stimulation in peripheral blood (PB) and lymph node (LN) as measured by CFSE dilution via flow cytometry during AC or DC (n = 1 each). **(D)** Killing curves showing elimination of autologous PB HIV peptide pulsed CD4$^+$ T cells by HIV peptide-expanded PB or LN CD8$^+$ T cells at the indicated effector:target (E:T) ratios during AC or DC (n = 1 each). AUC = area under curve.

Table 1:

Subject characteristics

		AC (*n* = 17)	DC (*n* = 17)	*p* (*test*)
Age (years; median, *IQR*)		43 (*12*)	51 (*13*)	0.17 (*unpaired t test*)
Sex (n, %)	*Male* *Female*	16 (*94*%) 1 (*6*%)	13 (*76*%) 4 (24%)	0.34 (*Fisher's exact*)
Race/Ethnicity (n, %)	*White, non-Hispanic* *Black, non-Hispanic* *White, Hispanic* *Multiracial*	13 (*76*%) 2 (*12*%) 1 (*6*%) 1 (*6*%)	13 (*76*%) 4 (*24*%) - -	0.66 (*Fisher's exact*)
Protective *HLA-B* alleles	[*B*14*, *B*27*, *B*52*, *B*57*] (n, %)	10 (*59*%)	10 (*59*%)	1.00 (*Fisher's exact*)
Baseline (T1) viral load (log_{10} copies/mL; median, *IQR*)		2.48 (0.54)	2.60 (0.86)	0.38 (*unpaired t test*)
Fold Δ log_{10} viral load (T3/T1; median, *IQR*)		1.11 (0.19)	1.00 (0.21)	0.02 (*unpaired t test*)
Baseline (T1) CD4 count (cells/mL; median, *IQR*)		682 (*334*)	794 (*199*)	0.36 (*unpaired t test*)
Fold Δ CD4 count (T3/T1; median, *IQR*)		0.89 (*0.32*)	0.87 (*0.25*)	0.84 (*Mann-Whitney*)

KEY RESOURCES TABLE

REAGENT or RESOURCE	SOURCE	IDENTIFIER
Antibodies		
BUV395-conjugated anti-CD8 (clone RPA-T8)	BD Biosciences	Cat# 563795 RRID: AB_2722501
APC/Cy7-conjugated anti-CD45RA (clone HI100)	Biolegend	Cat# 304128 RRID: AB_10708880
FITC-conjugated anti-CD62L (clone DREG-56)	Biolegend	Cat# 304804 RRID: AB_314464
BV605-conjugated anti-PD1 (clone EH12.2H7)	Biolegend	Cat# 329924 RRID: AB_2563212
AlexaFluor 488 anti-TIM3 (clone 344823)	R&D Systems	Cat# FAB2365G RRID: AB_10719134
PE/Dazzle 594 anti-TIGIT (clone A15153G)	Biolegend	Cat# 372716 RRID: AB_2632931
PE/Cy7-conjugated anti-CD160 (clone BY55)	Biolegend	Cat# 341212 RRID: AB_2562876
PerCP/Cy5.5-conjugated anti-2B4 (clone C1.7)	Biolegend	Cat# 329516 RRID: AB_10919138
BV650-conjugated anti-CD39 (clone TU66)	BD Biosciences	Cat# 563681 RRID: AB_2738370
BV510-conjugated anti-CD57 (clone HNK-1)	Biolegend	Cat# 393314 RRID: AB_2750342
APC/Cy7-conjugated anti-CD28 (clone CD28.2)	Biolegend	Cat# 302966 RRID: AB_2800753
AlexaFluor 700-conjugated anti-CD3 (clone SK7)	Biolegend	Cat# 344822 RRID: AB_2563420
BV711-conjugated anti-CD107A (clone H4A3)	Biolegend	Cat# 328640 RRID: AB_2565840
PE-Cy7-conjugated anti-IFN-γ (clone B27)	Biolegend	Cat# 506518 RRID: AB_2123321
PerCP/Cy5.5 anti-TNF-α (clone Mab11)	Biolegend	Cat# 502926 RRID: AB_2204081
PE-conjugated anti-perforin (clone B-D48)	Biolegend	Cat# 353304 RRID: AB_2616860
PE/CF594 anti-granzyme B (clone GB11)	BD Biosciences	Cat# 562462 RRID: AB_2737618
BV605-conjugated anti-IL-2 (clone MQ1-17H12)	Biolegend	Cat# 500332 RRID: AB_2563877
BV605-conjugated anti-CD3 (clone SK7)	Biolegend	Cat# 344836 RRID: AB_2565825
BV711-conjugated anti-CD4 (clone RPA-T4)	Biolegend	Cat# 300558 RRID: AB_2564393
polyclonal goat anti-human IgD	Southern Biotech	Cat# 2030-01 RRID: AB_2795623
polyclonal rabbit anti-human CD8	Abcam	Cat# ab4055 RRID: AB_304247
Ultra-LEAF purified anti-CD3 (clone OKT3)	Biolegend	Cat# 317326 RRID: AB_11150592
Ultra-LEAF purified anti-CD28 (clone CD28.8)	Biolegend	Cat# 302934 RRID: AB _11148949
Chemicals, Peptides, and Recombinant Proteins		
Live/Dead Violet viability dye	Thermo Fisher	Cat# L34964
Live/Dead Near-IR viability dye	Thermo Fisher	Cat# L10119
CellTrace Far Red dye	Thermo Fisher	Cat# C34564
CellTrace Violet dye	Thermo Fisher	Cat# C34557
CellTrace CFSE dye	Thermo Fisher	Cat# C34554
Recombinant human interleukin-2 (IL-2)	Peptrotech	Cat# 200-02
GolgiStop	BD Biosciences	Cat# 554724
GolgiPlug	BD Biosciences	Cat# 555029
Cytofix	BD Biosciences	Cat# 554655
Cytofix/Cytoperm	BD Biosciences	Cat# 554722
pHLA monomers	ImmunAware	Cat# MHC-I Custom

REAGENT or RESOURCE	SOURCE	IDENTIFIER
APC-conjugated streptavidin	Biolegend	Cat# 405207
HLA-optimal HIV peptides	MGH peptide core facility	N/A
CMV, EBV and IAV peptide pool	Mabtech	Cat# 3618-1
Critical Commercial Assays		
EasySep Human CD8+ T Cell Isolation Kit	StemCell Technologies	Cat# 17953
EasySep Human CD8 Positive Selection Kit II	StemCell Technologies	Cat# 17853
EasySep Human CD4+ T Cell Isolation Kit	StemCell Technologies	Cat# 17952
Qiaamp Viral RNA Mini kit	Qiagen	Cat# 52904
SuperScript III One-Step RT-PCR System with Platinum™ *Taq* High Fidelity DNA Polymerase	Thermo Fisher	Cat# 12574030
Platinum™ *Taq* DNA Polymerase High Fidelity	Thermo Fisher	Cat# 11304029
MiSeq Reagent Kit v2 500 Cycle Kit	Illumina	Cat# MS-102-2003
Allprep DNA/RNA Micro Isolation Kit	Qiagen	Cat# 80284
SuperScript II Reverse Transcriptase	Thermo Fisher	Cat# 18064071
KAPA HiFi HotStart ReadyMix	Roche	Cat# KK2602
Nextera XT Tagmentation Kit	Illumina	Cat# FC-131
NextSeq 500/550 High Output v2.5 150-Cycle Kit	Illumina	Cat# 20024907
RNAScope Multiplex Fluorescent Reagent Kit v2	Advanced Cell Diagnostics	Cat# 323100
Deposited Data		
HIV sequencing data	This paper	Genbank: MW924797-MW924814
RNA-sequencing data	This paper	GEO: GSE168296
LCMV microarray data	Doering et al., 2012	GEO: GSE41867
HIV controller and progressor microarray data	Quigley et al., 2010	GEO: GSE24082
Metastatic melanoma microarray data	Baitch et al., 2011	GEO: GSE24536
Oligonucleotides		
Cy5-conjugated HIV *gagpol* probe	Advanced Cell Diagnostics	Cat# 317698
Software and Algorithms		
limma	Ritchie et al., 2015	RRID:SCR_010943
Vicuna	Yang et al., 2012	RRID:SCR_006302
Vprofiler	Henn et al., 2012	broadinstitute.org/viral-genomics/v-profiler
Mosaik	Lee et al., 2014	RRID:SCR_005486
V-Phaser 2	Yang et al., 2013	RRID:SCR_005212
SeaView	Gouy et al., 2010	RRID:SCR_015059
muscle	Edgar, 2004	RRID:SCR_011812
PhyML	Guindon et al., 2010	RRID:SCR_014629
RSEM	Li and Dewey, 2011	RRID:SCR_013027
DESeq2	Love et al., 2014	RRID:SCR_015687
GSVA	Hänzelmann et al., 2013	bioconductor.org/packages/release/bioc/html/GSVA.html
MiXCR	Bolotin et al., 2015	RRID:SCR_018725